UNIVERSITY OF JYVÄSKYLÄ

Removal of alkylthiols from gold surface: Molecular dynamics simulations in density functional theory

Sami J. Kaappa
University of Jyväskylä, Department of Physics

Master's thesis
sami.j.parviainen@student.jyu.fi
February 16, 2015
Advisors: Sami Malola,
Pekka Koskinen,
Hannu Häkkinen

Acknowledgements

Most of the calculations performed in this study were run at Sisu supercomputer of IT Center for Science (CSC, Center of Scientific Computing). I also thank my advisors for professional and enthusiastic aid and support during the work.

Abstract

Self-assembled monolayers (SAMs) are systems of organic compounds adsorbed onto metal or silicon, forming a dense cover on top of the substrate; the most studied system of SAMs consists of alkylthiols on gold surface. In 2012, Liao *et al.* [1] found out, as a side-product of their chemical lift-off lithography research, that when the thiol cover was pulled off the gold surface, a layer of gold was also removed from the substrate. In our study, this process was simulated using density functional theory (DFT) within projector augmented-wave (PAW) method to examine the dynamics at the interface of gold and the thiol cover. According to our results, acquired using the linear combination of atomic orbitals (LCAO) method and the PBE functional, about half of the top layer of gold is removed from the surface by the thiols. Both planar Au(111) surface and a surface with a terrace, Au(332), were examined and they showed similar behavior during the process. As this kind of calculations have not been performed before, some parameter tests including the pulling speed and the Langevin friction parameter tests were run. I also performed some calculations considering the optimal geometries and energetics of different alkylthiols and ensured that the LCAO method is justified in the dynamics simulations; the results were in agreement with the literature values. This study sheds light to the physical and chemical phenomena at the interface of gold surface and alkylthiol monolayers and builds a base for further investigations on the subject.

Contents

1 Introduction

Noble and coinage metal surfaces have shown great potential as nanometer-sized laboratories in material sciences and molecule research in biochemistry, for they are relatively stable and easy to control. However, their stability and purity suffers from the atmospheric molecules such as sulfur oxides and nitrogen oxides which react with the surface and oxidize it. Although this happens slowly, they quickly become dirty in a sense that the surface does not have the properties of interest anymore. A widely known way to alter the physical, chemical and electronic properties of metal surfaces is the use of self-assembled monolayers (SAM). SAMs consist of organic molecules which, let in contact with the surface, assemble onto it symmetrically and densely, forming a coat that thoroughly covers the surface [1, 2, 3]. The most studied system consists of gold surface with sulfur-based SAMs because thiols are observed to bind strongly to gold surfaces and the organic thiol molecules are also stable and easy to prepare [4]. One of the great aspects of SAMs is also the possibility to tailor the organic molecule in question. For example, the length of the carbon chain can be varied in alkanethiols, and the end group of the alkanethiol can also be changed to achieve different behaviour of the new organic surface that forms above the SAM.

The variety of applications implementing SAMs is vast. Probably the most noticeable impact it has had on biochemistry and biomedical sciences, for the method offers a low-cost and easy way to mimic biological surfaces and interfaces, such as the cell wall [5]. The SAMs therefore form a nanosized laboratory where the interactions and phenomena of organic molecules and surfaces can be studied. Self-assembled monolayers have also been used to cover metal systems with other symmetries: for example, Haes and Van Duyne showed that different amino acids assembled to silver nanotriangles have different contribution to the plasmonic features of the system [6], and by comparing the optical spectra of the systems one can detect and recognize different amino acids and proteins. One benefit of this recognition method is that the sample size can be very small; the amount of molecules under investigation can be measured in numbers of molecules rather than in molarity. In fact, it is quite a widely used method to attach organic molecules onto

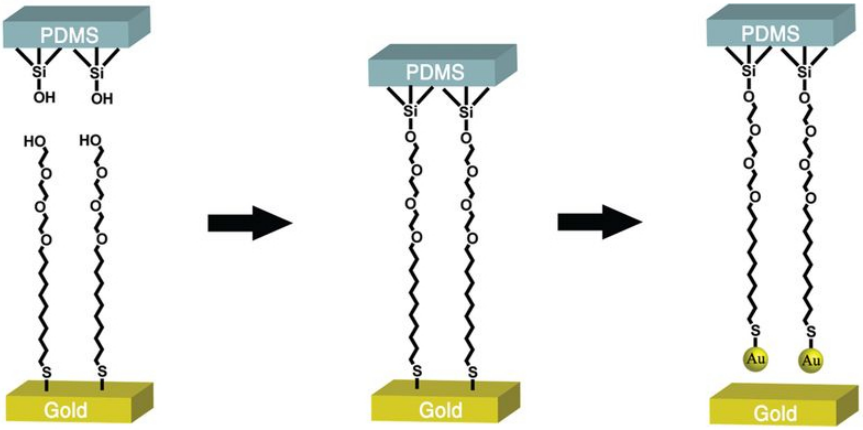

Figure 1: The idea of chemical lift-off lithography. The two SAMs are brought in contact to bind to each other. While separating the substrates, the thiolates of the lower SAMs are removed together with some gold originating at the other substrate. The figure origins at ref. [1].

nanoparticles so that the molecules form a shielding shell around the particles; the most important effect here is the stabilizing effect of the monolayer that prevents the nanoparticles from aggregating and decomposing in solution [7, 8]. In a similar manner as the triangular nanosilver, the SAM-protected clusters are often used to detect organic molecules via methods that are based on the effect of the monolayer on the optical behaviour of the particles [9]. An example of this kind of method was introduced by Elghanian *et al.* who managed to detect polynucleotides using DNA-assembled gold nanoparticles [10]. A similar method was used by Liu and Lu who presented a method to detect and quantify metal ions in solution [11]. Outside the detection applications, other kinds of biomedical applications exist too. For example, Salem *et al.* used Au/Ni rods to transfer DNA into cells by attaching certain protein molecules to the golden part of the rod and DNA to the nickel part [12]. While the protein is thus accepted to enter the cell through the cell wall, the rod is also fully transferred inside, still carrying the DNA and is thus able to modify the genetics of the cell.

This master's thesis is closely related to another application considering the self-assembled monolayers, namely lithography. In 2012, Liao *et al.* represented a new method to improve the convenience and fabrication rate compared to old methods [1]. In the method, conventional lithography methods are first used to

pattern a functionalized SAM on the stamp chip. This stamp is then placed on top of another SAM-covered gold substrate (mostly alkanethiols were used) to contact the functionalized SAM molecules of the stamp to the monolayer of the lower substrate, see fig. 1. The SAM molecules react and bind to each other with covalent bonds, and when the stamp is removed, the reacted molecules are pulled off the surface and thus the pattern is transferred to the lower monolayer as a negative copy. Because the stamp can be cleaned, it can be used multiple times and thus the method is many times faster than the conventional methods such as the electron beam lithography (EBL) where the patterning is quite slow and energy-consuming due to the scanning time and the need of vacuum. This kind of lithography could be used in, for example, research done by Singhvi *et al.*, who have utilized the older methods to create a patterned monolayer on gold surface and to attach entire cells onto them in order to study their behaviour in fixed positions and conditions [13].

The method of Liao *et al.* is called chemical lift-off lithography (CLL). While investigating the stamp substrate after the procedure with X-ray photoelectron spectroscopy (XPS), they noticed that there exists some gold in addition to the organic SAM molecules, meaning that some gold is removed from the substrate surface while removing the stamp. This thesis reports the computational *ab initio* study considering the molecular dynamics at the surface of gold while the thiols are pulled off. The aim of this work is to get theoretical understanding of the physical and chemical phenomena that drives the observed rip-off of thiols and gold molecules from the gold surface.

2 Theory and computational methods

In the computational part of the work, the density functional theory (DFT) was used with the projector-augmented wave method (PAW) for structural optimization and molecular dynamics. The PAW method was used through the code named Grid PAW (GPAW) [14, 15], which uses the Atomistic Simulation Enviroment (ASE) [16]. Before going to the details of those computational methods, some basic information about the physics and chemistry of gold and self-assembled monolayers is given.

2.1 Chemistry of gold and thiols

As mentioned in chapter 1, there are many structures where the bond between gold and sulfur plays the dominant role, for example SAMs, thiol-covered gold nanoparticles and polymeric molecules where there are repeating units that contain Au-S bonds. The nature of the bond in question is often discussed due to its high stability, which is interesting while gold is known to be chemically inert in bulk form. The binding of Au-S is not trivial, as the formalism needs to take the relativistic effects into account to deal with the electron orbitals of gold; the relativistic effects affect the extension of the orbitals of gold and interactions between them [17]. However, the relativity is easily implemented in the calculations, and thus some progress has been made. For example, in ring-like structures, the sp^3 hybridization of sulfur is known to bound to sp^3 hybridized orbitals and the 5d orbital of gold (sulfur atom has electron configuration of $[Ne]3s^23p^4$ and gold has $[Xe]4f^{14}5d^{10}6s^1$) and the oxidation state of gold is +I [18].

In the present study, however, surface structures and self-assembled monolayers (SAMs) were investigated. A SAM is simply a close-packing cover of organic molecules on top of metal or silicon substrate, and alkanethiols are known to form stable monolayers on gold surfaces [19, 17]; the bond strength between alkanethiols and gold surface has been determined to values around 1.8 eV [4, 20]. An example of a thiolate monolayer is shown in figure 2. What currently is not so simple is the structure and birth mechanism of the monolayers. A couple of decades ago,

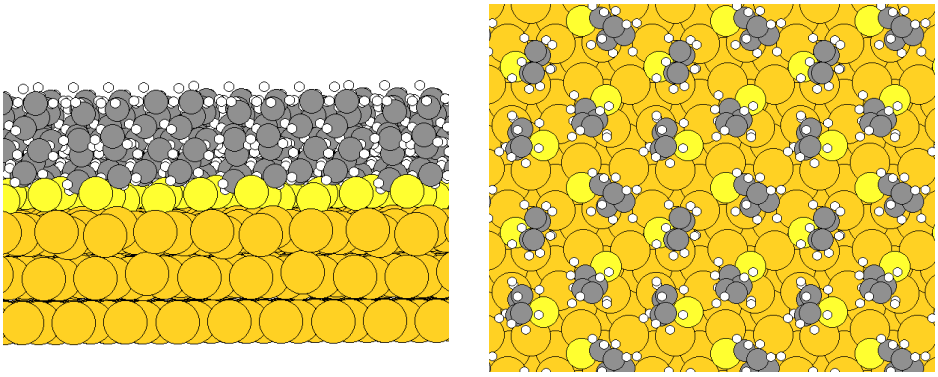

(a) (b)

Figure 2: An example of $(\sqrt{3}\times\sqrt{3})$R30° structured high-coverage self-assembled monolayer consisting of SC_4H_9 molecules on top of Au(111) surface. (a) The structure shown from side. (b) The same structure shown from top of the surface.

the alkanethiols were suggested to bind to hollow sites of the Au(111) surface atoms with the orientation of carbon chains to either straight up or with the angle 59° from the Au plane (corresponding to sp and sp^3 bonding, respectively) with the high-coverage structure being $(\sqrt{3}\times\sqrt{3})$R30° [4]. Later, it was shown computationally that energetically the most favourable site for the thiol is hollow-bridge site with the tilt angle of S-C bond of around 50° [21, 22].

In 2006, however, Maksymovych *et al.* published results which suggest that the thiols anchor to the a-top positions bound to gold adatoms (two thiols per adatom) lying at the bridge sites, the unit cell having the structure c(4 × 2) [23, 19]. The use of these RS-Au-SR units in the models fix multiple problems experienced in determining the structure of the thiol SAMs [20]. At present, it is still unclear how these adatom units are formed: How do the gold adatoms get there, on top of the surface, considering pure Au(111) surface or surface with terraces as the initial structure? In any case, it is known that as the thiol molecules H-SR are adsorbed onto gold surface, they prefer to follow the reaction path

$$2\ \text{H-SR} + \text{Au(surface)} \rightarrow \text{H}_2 + 2\ \text{RS-Au(surface)}, \qquad (1)$$

meaning that the thiol is in fact adsorbed as thiolate, releasing the hydrogen. The other alternative would be that the H-SR is bound to gold as such via lone-

pair electrons of sulfur, but this process is energetically less favourable compared to the thiyl radical adsorption [17]. Thus, thiolates are used in my calculations considering the adsorption to hollow-bridge sites of gold.

2.2 Density functional theory

The density functional theory (DFT) is a widely used *ab initio* method to calculate the ground state properties of an atomistic system. The history of the density functional theory is said to be started in 1964 when Hohenberg and Kohn introduced their improvements on Thomas-Fermi methods [24]. The traditional Thomas-Fermi model proceeds by taking into account only the classical interactions between electrons and presenting the kinetic energy of the electrons as the one of uniform electron gas [25], whereas the modern DFT can handle these phenomena much more accurately. In this section, I will present the most important and essential steps and assumptions in deriving the equations needed to implement DFT in work, but I will not derive them in details. Most of the progress here uses the book by Parr and Yang (ref. [26]) as reference.

2.2.1 The Schrödinger equation

We begin the derivation of DFT by introducing the stationary Schrödinger equation

$$\hat{H}\Psi(\vec{r}_1, \vec{r}_2, \ldots, \vec{r}_N, s_1, s_2, \ldots, s_N) = E\Psi(\vec{r}_1, \vec{r}_2, \ldots, \vec{r}_N, s_1, s_2, \ldots, s_N) \qquad (2)$$

of an atomic system with N electrons with positions $\vec{r}_i$ and spin numbers s_i. According to the equation (2), the eigenvalues of the Hamiltonian operator $\hat{H}$ are the electronic energy states E of the system and its eigenvectors are the probability amplitude matrices Ψ. If the wave functions Ψ are normalized, the expectation

value of an energy measurement of the system is

$$\begin{aligned} E[\Psi] &= \langle \Psi | \hat{H} | \Psi \rangle \\ &= \int \Psi^* \hat{H} \Psi \mathrm{d}\vec{r}_1 \mathrm{d}\vec{r}_2 \ldots \mathrm{d}\vec{r}_N \mathrm{d}s_1 \mathrm{d}s_2 \ldots \mathrm{d}s_N, \end{aligned} \tag{3}$$

where the brackets indicate that E is a functional of Ψ. This simply means that E is a function of a function Ψ, not a function of a number.

Because an electron system certainly has a minimum energy corresponding to the occupation of electrons on certain energy levels obeying the Pauli exclusion principle, one of the expectation values of the Hamiltonians describing the system must be the lowest of them all. The lowest value is denoted as E_0 and the relation

$$E_0 \leq E[\Psi] \tag{4}$$

is called the variational principle; this is derived in, for example, ref. [26]. Put simple, the density functional theory is a method to find an approximate value for this ground state energy E_0, that is, to minimize the expectation value of the Hamiltonian as

$$E_0 = \min \left(\langle \Psi | \hat{H} | \Psi \rangle \right). \tag{5}$$

In principle, going through all the possible Hamiltonians that could describe the system (having the correct number of electrons N and the correct external potential) one would finally find the ground state and the corresponding properties, but trying that would not be sensible due to the number of variables and the fact that the exact form of the interaction potential is not known.

Let us look inside the Hamiltonian that describes the atomic system. In general, it consists of two terms: the kinetic energy operator $\hat{T}$ and the potential energy operator $\hat{V}$, that is

$$\hat{H} = \hat{T} + \hat{V}. \tag{6}$$

The kinetic energy of the system consists of the kinetic energy of the nuclei and of

the electrons. However, according to the Born-Oppenheimer approximation, the kinetic energy of the nuclei can be separated from the electrons' kinetic energy, for they do not interact with each other [27]. The total kinetic energy operator

$$\hat{T} = \hat{T}_{electrons} \tag{7}$$

is thus given solely by the kinetic energy operator for electrons, having the form

$$\hat{T}_{electrons} = -\frac{1}{2}\sum_i \nabla_i^2 \tag{8}$$

while atomic units are used; this is the case throughout this discussion. The potential energy can also be divided into Coulombic and non-Coulombic interactions as

$$\hat{V} = \hat{V}_{nn} + \hat{V}_{ee} + \hat{V}_0, \tag{9}$$

where V_{nn} is the Coulombic potential between nuclei, V_{ee} is the Coulombic potential between electrons and V_0 includes the external potential (external to electrons, eg. Coulomb interaction between nuclei and electrons). Again, the potential energy between two nuclei can be regarded as constant, so it can be neglected for now and added to the total energy in the end. The Coulombic electron-electron interaction operator in terms of the electron positions is given by

$$\hat{V}_{ee} = \sum_i^N \sum_j^N 1/r_{ij} \tag{10}$$

where r_{ij} is the distance between the electron positions. The rest of the potential, including the interaction between nuclei and electrons, is given by

$$\hat{V}_{ne} = \sum_i^N \hat{V}_{ext}(\vec{r}_i), \tag{11}$$

where $\hat{V}_{ext}(\vec{r}_i)$ is the external potential at electron position $\vec{r}_i$. To sum up, the Hamiltonian for electrons in a system with N electrons and with the external

potential V_{ext} becomes

$$\hat{H} = -\frac{1}{2}\sum_{i}^{N}\nabla_i^2 + \sum_{i}^{N}V_{ext}(\vec{r}_i) + \sum_{i}^{N}\sum_{j}^{N}1/r_{ij}, \tag{12}$$

where the summing indices run over all the electrons.

2.2.2 Hartree-Fock method

Following the Hartree-Fock (HF) method, the ancestor of DFT, we assume that the wave function Ψ can be written in terms of N orthonormal spin orbitals χ_i that each represent a single electron [28]. Because electrons are fermions, the total wave function must meet the requirement of antisymmetry, that is, if two electrons are interchanged, the wave function is multiplied by -1. That is, in mathematics,

$$\Psi(\chi_1, \chi_2, \ldots, \chi_i, \ldots, \chi_j, \ldots, \chi_N) = -\Psi(\chi_1, \chi_2, \ldots, \chi_j, \ldots, \chi_i, \ldots, \chi_N). \tag{13}$$

Because the Hamiltonian of equation (12) does not take into account the requirement for antisymmetry, the normalized Slater determinant [29]

$$\Psi_0(\vec{x}_1, \vec{x}_2, \ldots, \vec{x}_N) = \frac{1}{\sqrt{N!}}\begin{vmatrix} \chi_1(\vec{x}_1) & \chi_2(\vec{x}_1) & \chi_3(\vec{x}_1) & \ldots & \chi_N(\vec{x}_1) \\ \chi_1(\vec{x}_2) & \chi_2(\vec{x}_2) & \chi_3(\vec{x}_2) & \ldots & \chi_N(\vec{x}_2) \\ \ldots & \ldots & \ldots & \ldots & \ldots \\ \chi_1(\vec{x}_N) & \chi_2(\vec{x}_N) & \chi_3(\vec{x}_N) & \ldots & \chi_N(\vec{x}_N) \end{vmatrix} \tag{14}$$

is introduced as an initial guess for the wave function Ψ; the determinant is clearly antisymmetric by the general properties of determinants. In equation (14), the orthonormal spin orbitals χ_i are functions of $\vec{x}_j$ that consist of spatial orbitals $\vec{\phi}_j$ and the spin function s_j. Therefore, this form of the wave function also includes the Pauli principle, since the orbitals must be linearly independent (otherwise the determinant would be equal to zero leading to no solution) so that if an orbital χ_i includes the same spatial orbital $\vec{\phi}_j$ as some other orbital χ_k, they must differ by their spin functions. In HF method, an approximation is done where a single

Slater determinant is assumed to be the solution of the Schrödinger equation. If we calculate the expectation value of the Hamiltonian (eq. (12)) in the state Ψ_0, the function to be minimized in equation (5) becomes [26]

$$E_{HF} = \sum_i H_i + \frac{1}{2}\sum_{i,j}(J_{ij} - K_{ij}), \tag{15}$$

where

$$H_i = \int \chi_i^*(\vec{x})[-\frac{1}{2}\nabla^2 + V_{ext}(\vec{x})]\chi_i(\vec{x})\mathrm{d}\vec{x}, \tag{16}$$

$$J_{ij} = \int\int \chi_i(\vec{x}_1)\chi_i^*(\vec{x}_1)\frac{1}{r_{12}}\chi_j^*(\vec{x}_2)\chi_j(\vec{x}_2)\mathrm{d}\vec{x}_1\mathrm{d}\vec{x}_2 \text{ and} \tag{17}$$

$$K_{ij} = \int\int \chi_i^*(\vec{x}_1)\chi_j(\vec{x}_1)\frac{1}{r_{12}}\chi_i(\vec{x}_2)\chi_j^*(\vec{x}_2)\mathrm{d}\vec{x}_1\mathrm{d}\vec{x}_2 \tag{18}$$

hold. Taking into account the orthonormality of the spin orbitals χ_i, the minimizing then leads to the Hartree-Fock equations [26, 27]

$$\hat{f}_i\chi_i = \epsilon_i\chi_i, \tag{19}$$

where ϵ_i is interpreted as the orbital energy and $\hat{f}_i$ is defined as

$$\hat{f}_i = -\frac{1}{2}\nabla_i^2 + \hat{V}_{ext} + \hat{V}_{HF}(i). \tag{20}$$

In equation (20), the Hartree-Fock potential $\hat{V}_{HF}$ is given by

$$\hat{V}_{HF}(\vec{x}_1) = \sum_j (\hat{J}_j(\vec{x}_1) - \hat{K}_j(\vec{x}_1)), \tag{21}$$

where

$$\hat{J}_j(\vec{x}_1) = \int |\chi_j(\vec{x}_2)|^2\frac{1}{r_{12}}\mathrm{d}\vec{x}_2 \text{ and} \tag{22}$$

$$\hat{K}_j(\vec{x}_1)\chi_i(\vec{x}_1) = \int \chi_j^*(\vec{x}_2)\frac{1}{r_{12}}\chi_i(\vec{x}_2)\mathrm{d}\vec{x}_2\chi_j(\vec{x}_1). \tag{23}$$

2.2.3 Electron density and Hohenberg-Kohn theorems

To ease the calculations utilizing the Hartree-Fock method, Hohenberg and Kohn introduced the idea, a derivative of the Thomas-Fermi method, that electron systems can be also described in terms of electron density $\rho(\vec{r})$ instead of the universal positions of the electrons [24]. In general, the electron density in certain position $\vec{r}_1$ is intuitively defined as

$$\rho(\vec{r}_1) = N \int \dots \int |\Psi(\vec{x}_1, \vec{x}_2, \dots, \vec{x}_N)|^2 \mathrm{d}s_1 \mathrm{d}\vec{x}_2 \mathrm{d}\vec{x}_3 \dots \mathrm{d}\vec{x}_N, \tag{24}$$

where $\vec{x}_i = \vec{r}_i \times s_i$ and where $|\Psi(\vec{x}_1, \vec{x}_2, \dots, \vec{x}_N)|^2 \mathrm{d}\vec{x}_i$ gives the probability of finding an electron in differential position $\mathrm{d}\vec{x}_i$. Due to the conservation of electrons in the system, it also holds that

$$N = \int \rho(\vec{r}) \mathrm{d}\vec{r}. \tag{25}$$

With these facts, Hohenberg and Kohn presented two theorems which later led to the birth of the Kohn-Sham method and the density functional theory. The first theorem states that the external potential is a unique functional of the electron density distribution $\rho(\vec{r})$, and thus so is the ground state energy. The second theorem is nothing more than the variational principle in terms of the electron density. This can be put as

$$\begin{aligned} E[\rho] &= T[\rho] + V_{ne}[\rho] + V_{ee}[\rho] \\ &= \int \rho(\vec{r}) V_{ext}(\vec{r}) \mathrm{d}\vec{r} + F_{HK}[\rho], \end{aligned} \tag{26}$$

where

$$F_{HK}[\rho] = T[\rho] + V_{ee}[\rho] \tag{27}$$

is the one functional in DFT that contains everything that is not known exactly. Put differently, exact knowledge of $F_{HK}[\rho]$ would lead to the exact value for the ground state energy of the electron system. For consistency of notation, let us add

here that the terms in equations (26) and (27) represent the expectation values of the corresponding operators, for example, $T \equiv \langle\Psi|\hat{T}|\Psi\rangle$. The total energy E is naturally the expectation value of the Hamiltonian.

2.2.4 Kohn-Sham method

In 1965, a year after the revolutionary findings of Hohenberg and Kohn, Kohn and Sham built a method that the modern DFT strongly leans on [30]. In the method, the known and the unknown terms of the kinetic energy and the electron-electron interaction are separated as

$$F[\rho] = T_s[\rho] + J[\rho] + E_{xc}[\rho], \tag{28}$$

where

$$E_{xc}[\rho] = (T[\rho] - T_s[\rho]) + (V_{ee}[\rho] - J[\rho]). \tag{29}$$

In equations (28) and (29), T_s is the kinetic energy of the system with no interactions between the electrons and J is the classical (*ie.* Coulombic) interaction between electrons. In equation (29), the first parenthesis contains the error in the kinetic energy T_s compared to the total kinetic energy, and the second parenthesis contains the nonclassical part of the electron-electron interaction. More details about the exchange-correlation energy E_{xc} are given in chapter 2.2.5.

Thus, the method describes a non-interactive system which is embedded in an external potential field that in the end contains the interaction potentials. The energy of a Kohn-Sham orbital χ_i is then given by the eigenvalues E_i of the equation

$$\begin{aligned} E_i\chi_i &= (\hat{T}_s[\rho] + \hat{J}[\rho] + \hat{V}_{ne}[\rho] + \hat{V}_{xc}[\rho])\chi_i \\ &= \Big(-\frac{1}{2}\nabla^2 + \int \frac{\rho(\vec{r}')}{|\vec{r} - \vec{r}'|}\mathrm{d}\vec{r}' + \int \rho(\vec{r})\hat{V}_{ext}(\vec{r})\mathrm{d}\vec{r} + \hat{V}_{xc}[\rho]\Big)\chi_i, \end{aligned} \tag{30}$$

where the electron density is calculated as

$$\rho(\vec{r}) = \sum_{i=1}^{N} \sum_{s} |\chi_i(\vec{r}, s)|^2. \tag{31}$$

Because the density and the wave functions are dependent on each other via equations (30) and (31), the problem must be solved iteratively. The procedure might go for example as follows:

1. Initial guess for wave functions based on some atomic basis is substituted to equation (31) which then gives an initial function for the density.
2. The density is substituted to equation (30) which gives the new wave functions (and the orbital energies)
3. The density function is calculated again using the new wave functions.
4. The differences between the old and the new wave functions and densities are calculated.
5. If the differences are below a given limit, the iterative calculation is ready (*ie.* convergence is achieved) and can be stopped. If not, the calculation is continued from stage 2.

This iterative procedure is called self-consisted field (SCF) cycle. After the procedure, all the properties of the system can be derived from the Kohn-Sham orbitals and the density. For example, the total energy of the system can be calculated via equations (26) and (28).

2.2.5 Exchange-correlation functionals V_{xc}

In equation (30), there exists an unknown term, V_{xc}, that is defined as

$$V_{xc} = \frac{\delta E_{xc}[\rho]}{\delta \rho(\vec{r})} \tag{32}$$

where E_{xc} is the exchange-correlation energy that contains the non-classical interaction energy between electrons and the difference between the kinetic energies of

the interacting and the non-interacting systems. The functional is usually separated to exchange and correlation terms that are independent of each other. The exchange energy is related to the fact that two parallel-spin electrons cannot have the same position and, therefore, they have some kind of non-classical interaction that can be defined as [26]

$$E_x[\rho_\uparrow, \rho_\downarrow] = -\frac{1}{2}\int\int \frac{1}{r_{12}}\left[|\rho_{\uparrow\uparrow}(\vec{r}_1, \vec{r}_2)|^2 + |\rho_{\downarrow\downarrow}(\vec{r}_1, \vec{r}_2)|^2\right]\mathrm{d}\vec{r}_1\mathrm{d}\vec{r}_2, \tag{33}$$

where

$$\rho_{\uparrow\uparrow}(\vec{r}_1, \vec{r}_2) = \sum_i n_{i\uparrow}\chi_{i\uparrow}(\vec{r}_1)\chi^*_{i\uparrow}(\vec{r}_2) \quad \text{and} \tag{34}$$

$$\rho_{\downarrow\downarrow}(\vec{r}_1, \vec{r}_2) = \sum_i n_{i\downarrow}\chi_{i\downarrow}(\vec{r}_1)\chi^*_{i\downarrow}(\vec{r}_2). \tag{35}$$

The factors $n_{i_\uparrow}$ and $n_{i\downarrow}$ are the occupation numbers of the Kohn-Sham orbitals $\chi_{i\uparrow}$ and $\chi_{i\downarrow}$ with the corresponding spin function $\uparrow$ or $\downarrow$, respectively. The correlation term cannot be given a similar expression, and so it is simply defined as the difference of the total energy and the energy resulting from the known origins:

$$E_c = E - (T_s + J + V_{ne} + E_x). \tag{36}$$

As one can assume from the previous discussion, the expression of E_{xc} has been and still remains the greatest difficulty in DFT [26]; although, many ways to describe this functional have been developed. The first and the most simple functional was represented already by Hohenberg and Kohn in 1964 [24], namely the local density approximation (LDA). In LDA, the exchange-correlation contribution is given by

$$E_{xc}^{LDA}[\rho] = \int \rho(\vec{r})\epsilon_{xc}(\rho)\mathrm{d}\vec{r}, \tag{37}$$

where ϵ_{xc} is defined as the exchange-correlation energy per electron in uniform, non-interacting electron gas. The term can be divided in the exchange and corre-

lation parts as

$$\epsilon_{xc}(\rho) = \epsilon_x(\rho) + \epsilon_c(\rho) \tag{38}$$

of which the exhange part ϵ_x was already derived by Dirac in 1930 [31] and has the form

$$\epsilon_x(\rho) = \frac{3}{4}\Big(\frac{3}{\pi}\Big)^{1/3}(\rho(\vec{r}))^{1/3}. \tag{39}$$

The correlation part ϵ_c in the LDA approach has, in turn, a wider variety of expressions in literature due to its troublesome complexity. By default, GPAW uses an expression by Perdew and Wang [32]. They implemented a spin-interpolation formula that was presented by Vosko, Wilk and Nusair in 1980 [33], which is given in terms of the density parameter r_s

$$r_s = [3/4\pi(\rho_\uparrow + \rho_\downarrow)]^{1/3} \tag{40}$$

and the spin polarization

$$\zeta = \frac{\rho_\uparrow - \rho_\downarrow}{\rho_\uparrow + \rho_\downarrow}. \tag{41}$$

The subscripts $\uparrow$ and $\downarrow$ represent antiparallel spin numbers. The correlation energy per particle is then given by

$$\epsilon_c(r_s, \zeta) = \epsilon_c(r_s, 0) + \alpha_c(r_s)\frac{f(\zeta)}{f''(0)}(1 - \zeta^4) + [\epsilon_c(r_s, 1) - \epsilon_c(r_s, 0)]f(\zeta)\zeta^4, \tag{42}$$

where

$$f(\zeta) = \frac{(1+\zeta)^{4/3} + (1-\zeta)^{4/3} - 2}{2^{4/3} - 2}. \tag{43}$$

In the method of Perdew and Wang, the terms $\epsilon_c(r_s, 0)$, $\epsilon_c(r_s, 1)$ and $\alpha_c(r_s)$ are

approximated by optimizing multiple parameters to minimize the function

$$G(r_s, A, \alpha_1, \beta_1, \beta_2, \beta_3, \beta_4, p) = -2A(1+\alpha_1 r_s)\times \\ \ln\Big[1+(2A(\beta_1 r_s^{1/2}+\beta_2 r_s+\beta_3 r_s^{3/2}+\beta_4 r_s^{p+1})^{-1}\Big]. \quad (44)$$

The fact that the exchange-correlation energy here depends only on the value of electron density in position $\vec{r}$ makes this approximation very coarse, which is therefore not applicable in calculating single atoms or molecules where the electron density varies remarkably in space. For that purpose, the functionals that make use of generalized gradient approximations (GGA) are used to achieve higher accuracy.

The idea of GGA was also introduced already by Hohenberg and Kohn [24] as they suggested that the residual energy functional (*ie.* the exchange-correlation functional in Kohn-Sham method) can be expanded so that it, in addition to the *value* of the electron density, takes into account the *gradient* of it. That is,

$$E_{xc}^{GGA}[\rho] = \int f(\rho, \nabla\rho)\mathrm{d}\vec{r}, \quad (45)$$

where f is some (local) function of the density and its gradient. In my calculations, the evaluation of f was given by Perdew, Burke and Ernzerhof [34], after whom this PBE functional is named. In the method, the exchange-correlation energy is again separated to exchange and correlation parts that contain the forms of ϵ_x and ϵ_c of the LDA theory (equations (39) and (42)). The correlation part is then given by

$$E_C^{GGA}[\rho] = \int \rho\big[\epsilon_c(r_s,\zeta)+H(r_s,\zeta,t)\big]\mathrm{d}\vec{r}, \quad (46)$$

where t is a density gradient, given as

$$t = \frac{|\nabla\rho|}{2\phi k_s \rho}. \quad (47)$$

In equation (47), the spin-scaling factor ϕ is given by

$$\phi(\zeta) = \frac{1}{2}[(1+\zeta)^{2/3} + (1-\zeta)^{2/3}] \tag{48}$$

and the Thomas-Fermi screening wave number k_s can be written as

$$k_s = \sqrt{\frac{4m_e e^2 k_F}{\pi\hbar^2}}, \quad k_F = \sqrt[3]{3\pi^2\rho}. \tag{49}$$

Using the boundary conditions of slowly varying limit $t \to 0$, rapidly varying limit $t \to \infty$ and high-density limit, Perdew *et al.* [34] ended up with the form of H as

$$H = \frac{m_e e^4}{\hbar^2}\gamma\phi^3 \ln\Big(1 + \frac{\beta}{\gamma}t^2\frac{1+At^2}{1+At^2+A^2t^4}\Big), \tag{50}$$

where A has the form of

$$A = \frac{\beta}{\gamma}\Big[\exp\Big(-\frac{\epsilon_c\hbar^2}{\gamma\phi^3 m_e e^4}\Big) - 1\Big]^{-1}. \tag{51}$$

The factors β and γ are just numbers based on the boundary conditions and natural constants therein.

The exchange part of the functional is then given as

$$E_x[\rho_\uparrow, \rho_\downarrow] = \frac{1}{2}(E_x[2\rho_\uparrow] + E_x[2\rho_\downarrow]), \tag{52}$$

where $E_x[\rho_s]$ is defined as

$$E_x[\rho_s] = \int \rho_s \epsilon_x(\rho_s) F_X(s). \tag{53}$$

The factor $F_X(s)$ is called the spin-polarized enhancement factor, and considering the boundary conditions of linear response and the Lieb-Oxford bound, it may have the simple form of

$$F_X(s) = 1 + \kappa - \frac{\kappa^2}{\kappa + \mu s^2}, \tag{54}$$

where the variable s is another density gradient

$$s = \frac{|\nabla \rho|}{2k_F \rho} \tag{55}$$

and κ and μ are, again, dimensionless numbers, evaluated in the original publication of the method, ref. [34].

2.3 Projector-augmented wave method

In the chapter 2.2, the principles of the density functional theory were represented. However, to implement DFT efficiently one has to determine a reasonable initial basis for the Kohn-Sham wave functions and choose the functional to describe the exchange and correlation effects accurately enough. Also, it happens that the wave functions show very sharp features near the nuclei, as the electrons occupy the lowest atomic orbitals whose mathematical representations are orthogonal [35]. Further away, in the region of molecular bonding (and smaller electron density), the wave functions behave more smoothly. To accurately describe these rapid oscillations, one would have to use very fine computational grid so that the behaviour of the orbitals would not be chaotic. Eventually, this would be very frustrating because in most parts of the space the functions are smooth.

One way to overcome this problem is to use pseudopotentials which are embedded into the Hamiltonian to describe the oscillating parts of the wave functions, while the naturally smooth parts are left as they are [36].

In my studies, the Projector-augmented wave method (PAW) was used to eliminate for example the sharp-feature problem. In PAW, the Kohn-Sham wave functions (χ_i in equation (30)) are manipulated so that inside an atom-specific radius r_c, centered at a nucleus, the wave function is described to behave smoothly, and outside this augmentation sphere they act normally [35].

2.3.1 Wave function transform

In PAW, an operator $\hat{\mathcal{T}}$ is defined that maps an auxiliary wave function $\tilde{\chi}_i$ into the original Hilbert space as

$$|\chi_i\rangle = \hat{\mathcal{T}}|\tilde{\chi}_i\rangle. \tag{56}$$

The Schrödinger equation for the auxiliary wave functions is thus described as

$$\hat{\mathcal{T}}^\dagger \hat{H} \hat{\mathcal{T}} |\tilde{\chi}_i\rangle = E_i \hat{\mathcal{T}}^\dagger \hat{\mathcal{T}} |\tilde{\chi}_i\rangle. \tag{57}$$

To define the operation done by $\hat{\mathcal{T}}$, we first expand the Kohn-Sham orbitals and the auxiliary ones as

$$|\tilde{\chi}_i\rangle = \sum_q |\tilde{\phi}_q\rangle\langle p_q|\tilde{\chi}_i\rangle \quad \text{and} \tag{58}$$

$$|\chi_i\rangle = \hat{\mathcal{T}}|\tilde{\chi}_i\rangle = \sum_q |\phi_q\rangle\langle p_q|\tilde{\chi}_i\rangle, \tag{59}$$

where the partial waves ϕ_q and $\tilde{\phi}_q$ form bases of the Hilbert spaces each. The Kohn-Sham orbitals $|\phi\rangle$ are initially determined from the Kohn-Sham equations (equations (30) and (31)) and the auxiliary partial waves $|\tilde{\phi}\rangle$ are built so that they meet the required smoothness inside the augmentation sphere and are equal to $|\phi\rangle$ outside of it [35]. Because we want to modify the wave function only inside the augmentation sphere, we restrict the expansions (equations (58) and (59)) to the area where $|\vec{r} - \vec{R}_a| < r_c$ ($\vec{r}$ is the position vector, $\vec{R}_a$ is the position vector of the atom core in question and r_c is the radius of the augmentation sphere). The functions $|p_q\rangle$ that appear in the expansion coefficients are called smooth projector functions and they are defined as

$$\langle p_q| = \sum_j (\{\langle f_l|\tilde{\phi}_m\rangle\})^{-1}_{qj} \langle f_j|, \tag{60}$$

where the wave bracket notation indicates a matrix containing all the combinations of $\langle f_l|\tilde{\phi}_m\rangle$. The functions $|f_j\rangle$ are a complete set of linearly independent functions

that are to be chosen for the calculation. By the requirement of linearity of the transform operator $\hat{\mathcal{T}}$ and requiring no overlap between different augmentation spheres, the operator $\hat{\mathcal{T}}$ is finally written as [35]

$$\hat{\mathcal{T}} = 1 + \sum_i (|\phi_k\rangle - |\tilde{\phi}_k\rangle)\langle p_k|. \tag{61}$$

Now, the auxiliary wave functions $|\tilde{\phi}\rangle$ can be calculated via the Schrödinger equation (57) and the Kohn-Sham wave functions are derived from those as

$$|\chi_i\rangle = |\tilde{\chi}_i\rangle + \sum_k (|\phi_k\rangle - |\tilde{\phi}_k\rangle)\langle p_k|\tilde{\chi}_i\rangle \tag{62}$$

which is just the result of the operation $\hat{\mathcal{T}}|\tilde{\chi}_i\rangle$ (equations (56) and (61)).

2.3.2 The frozen core

As the chemical bonding occurs only by the interactions of valence electrons with the surrounding atoms and the valence electrons are relatively far from the atom nucleus, it is reasonable to make an approximation that the inner states are not altered very much in bonding compared to a free atom. This approximation can also be done in PAW: The core states that distribute only (or mostly) inside the augmentation spheres are left as they are while calculating the wave functions, that is, only the valence states are included in the expansions (equations (58) and (59)) of the wave functions. This approximation greatly reduces the need for computational resources as some of the states are left outside of the calculation.

2.3.3 Calculating measurable quantities in PAW

In the self-consistent field (SCF) cycle represented in the end of chapter 2.2.4, the wave functions are used to calculate the electron density, and therefore the density should be described in the terms of the auxiliary waves of the PAW method, too. By using equation (61) and canceling terms due to the properties of the waves inside and outside the augmentation region, one ends up with the description of a

general local operator in terms of the partial waves [35]:

$$\tilde{\hat{A}} = \hat{\mathcal{T}}^{\dagger}\hat{A}\hat{\mathcal{T}} \tag{63}$$

$$= A + \sum_{m,n} |p_m\rangle(\langle\phi_m|\hat{A}|\phi_n\rangle - \langle\tilde{\phi}_m|A|\tilde{\phi}_n\rangle)\langle p_n|. \tag{64}$$

When calculating expectation values for nonlocal operators, one has to add a term $\Delta\tilde{\hat{A}}$ to $\tilde{\hat{A}}$ that takes into account the nonlocality. According to Blöchl,

$$\Delta\tilde{\hat{A}} = \sum_m |p_m\rangle(\langle\phi_m| - \langle\tilde{\phi}_m|)A(1 - \sum_n |\tilde{\phi}_n\rangle\langle p_n|) + (1 - \sum_n |p_n\rangle\langle\tilde{\phi}_n|)A(|\phi_m\rangle - |\tilde{\phi}_m\rangle)\langle p_m|. \tag{65}$$

By calculating the expectation value of the density operator $|\vec{r}\rangle\langle\vec{r}|$ (which is a local operator) using equation (63), one arrives at

$$n(\vec{r}) = \sum_i f_i\langle\chi_i|\vec{r}\rangle\langle\vec{r}|\chi_i\rangle \tag{66}$$

$$= \tilde{n}(\vec{r}) + n_o(\vec{r}) - \tilde{n}_o(\vec{r}), \tag{67}$$

where f_i is the occupation number of the state χ_i and where [35]

$$\tilde{n}(\vec{r}) = \sum_i f_i\langle\tilde{\chi}_i|\vec{r}\rangle\langle\vec{r}|\tilde{\chi}_i\rangle, \tag{68}$$

$$n_o(\vec{r}) = \sum_{i,(m,n)} f_i\langle\tilde{\chi}_i|p_m\rangle\langle\phi_m|\vec{r}\rangle\langle\vec{r}|\phi_n\rangle\langle p_n|\tilde{\chi}_i\rangle, \tag{69}$$

and

$$\tilde{n}_o(\vec{r}) = \sum_{i,(m,n)} f_i\langle\tilde{\chi}_i|p_m\rangle\langle\tilde{\phi}_m|\vec{r}\rangle\langle\vec{r}|\tilde{\phi}_n\rangle\langle p_n|\tilde{\chi}_i\rangle. \tag{70}$$

The acquired density can then be used in the SCF-cycle. After convergence, one would like to calculate the total energy of the system. According to equations (26)

and (28), the total energy is calculated via

$$E[\rho] = T_s[\rho] + J[\rho] + V_{ne}[\rho] + E_{xc}[\rho], \tag{71}$$

where the terms represent the expectation values of the corresponding operators. Now that the classical kinetic energy T_s and the exchange-correlation energy E_{xc} are (semi-)local operators (E_{xc} in the case of LDA and GGA), their expectation values are given directly by equation (63). In contrast, the potential energy terms J and V_{ne} are clearly nonlocal operators and thus the nonlocal contribution of equation (65) has to be added to their local value. The corresponding equations are quite monstrous and can be read from, for example, the original PAW paper by Blöchl [35].

2.3.4 Linear combinations of atomic orbitals in PAW

In my molecular dynamics simulations, I used the linear combination of atomic orbitals (LCAO) method. When implementing the LCAO method in PAW, the wave functions defined in equation (56) are described as linear combinations of pre-defined atomic orbitals $\Phi_\mu(\vec{r})$ [37], that is

$$\tilde{\chi}_i(\vec{r}) = \sum_\mu c_{\mu i} \Phi_\mu(\vec{r}) \tag{72}$$

with the coefficients $c_{\mu i}$ that are to be determined to find the solution to the eigenvalue problem of the Hamiltonian. Thus, the problem becomes to find the coefficients $c_{\mu i}$ instead of directly seeking for the real-space wave functions. To construct the eigenvalue equation which is used to solve the coefficients, we define the overlap operator S as

$$S = \hat{\mathcal{T}}^\dagger \hat{\mathcal{T}} = 1 + \sum_{aij} |p_i^a\rangle \Delta S_{ij}^a \langle p_i^a|, \tag{73}$$

where

$$\Delta S_{ij}^a = \langle \phi_i^a | \phi_j^a \rangle - \langle \tilde{\phi}_i^a | \tilde{\phi}_j^a \rangle. \tag{74}$$

The matrix elements of the overlap integral are then described as [37]

$$\begin{aligned} S_{\mu\nu} &= \langle\Phi_\mu|S|\Phi_\nu\rangle \\ &= \langle\Phi_\mu|\Phi_\nu\rangle + \sum_{aij}\langle p_i^a|\Phi_\mu\rangle^* \Delta S_{ij}^a \langle p_j^a|\Phi_\nu\rangle. \end{aligned} \tag{75}$$

Re-writing the Schrödinger equation (57) gives now

$$\sum_\mu c_{\mu i}\hat{\tilde{H}}|\Phi_\mu\rangle = \sum_\mu c_{\mu i}\hat{S}|\Phi_\mu\rangle, \tag{76}$$

where the Hamiltonian $\hat{\tilde{H}}$ is defined as

$$\hat{\tilde{H}} \equiv \hat{\mathcal{T}}^\dagger \hat{H}\hat{\mathcal{T}}. \tag{77}$$

Using equation (61) for the transform operator $\hat{\mathcal{T}}$ we get

$$\hat{\tilde{H}} = -\frac{1}{2}\nabla^2 + \tilde{V} + \sum_{aij}|p_i^a\rangle \Delta H_{ij}^a \langle p_j^a|, \tag{78}$$

where $\tilde{V}$ is the potential energy of the system in terms of PAW method [37]. The matrix elements of the atomic Hamiltonians ΔH_{ij}^a can be regarded as

$$\Delta H_{ij}^a = \frac{\partial E}{\partial D_{ji}^a}, \tag{79}$$

that is, the derivative of the total energy with respect to the atomic density matrix elements

$$D_{ij}^a = \sum_{\mu\nu}\langle p_i^a|\Phi_\mu\rangle \rho_{\mu\nu}\langle p_j^a|\Phi_\nu\rangle, \tag{80}$$

where the density matrix $\rho_{\mu\nu}$ is defined as

$$\rho_{\mu\nu} = \sum_i c_{\mu i} f_i c_{\nu n}^*. \tag{81}$$

The matrix elements of the total Hamiltonian $\hat{\tilde{H}}$ are then given by

$$\begin{aligned}\tilde{H}_{\mu\nu} &\equiv \frac{\partial E}{\partial \rho_{\mu\nu}} \\ &= T_{\mu\nu} + V_{\mu\nu} + \sum_{aij} \langle p_i^a | \Phi_\mu \rangle \Delta H_{ij}^a \langle p_j^a | \Phi_\nu \rangle\end{aligned} \tag{82}$$

with the matrix elements of the kinetic energy T and the potential energy

$$T_{\mu\nu} = \langle \Phi_\mu | -\frac{1}{2}\nabla^2 | \Phi_\nu \rangle \quad \text{and} \tag{83}$$

$$V_{\mu\nu} = \int \Phi_\mu^*(\vec{r}) \tilde{V}(\vec{r}) \Phi_\nu(\vec{r}) \mathrm{d}\vec{r}. \tag{84}$$

Combining the equations (75), (76) and (82) we finally get the Schödinger equation for the LCAO method,

$$\sum_\nu H_{\mu\nu} c_{\nu i} = \sum_\nu S_{\mu\nu} c_{\nu i} E_i, \tag{85}$$

which gives the coefficients $c_{\nu i}$ that determine the Kohn-Sham wave functions in equation (72). Using the approximation that the wave functions can be written as linear combinations of atomic orbitals reduces the computational needs but, at the same time, some accuracy is sacrificed.

2.3.5 Basis sets

In LCAO, the wave functions were represented as linear combinations of the atomic orbitals, as described by the equation (72). The atomic orbitals must then be pre-calculated, and in PAW, it is done similarly as in the SIESTA method [38].

The atomic orbitals are written as products of the radial function $\varphi_{nl}(r)$ and a spherical harmonic $Y_{lm}(\vec{r})$, that is,

$$\Phi_{nlm}(\vec{r}) = \varphi_{nl}(r) Y_{lm}(\vec{r}). \tag{86}$$

While the spherical harmonics are generally well-known, the problem in determining the basis wave functions for each quantum number combination nlm is reduced

to seeking the radial functions $\varphi_{nl}(r)$. In the tight-binding method, introduced by Sankey and Niklewski (ref. [39]) and used in my calculations, the radial functions are set to zero beyond a certain, orbital-specific radius in order to reduce the number of calculation points. The first approximation for the radial function is then given by the (general) radial Schrödinger equation

$$\Big(-\frac{1}{2r}\frac{\mathrm{d}^2}{\mathrm{d}r^2} + \frac{l(l+1)}{2r^2} + V_l(r)\Big)\varphi_{nl}(r) = \epsilon_l \varphi_{nl}(r), \tag{87}$$

fulfilling the requirement $\varphi_{nl}(r_c) = 0$ where r_c is the tight-binding cutoff radius. $V_l(r)$ is the pseudopotential affecting the electrons and in my calculations its shape is given in reference [40].

Naturally, greater accuracy is achieved with increasing the amount of basis functions. In my calculations, this is obtained using the double-ζ basis set, where the basis is literally doubled so that the second-ζ basis wave functions have the same shape for the its tail (where $r \to r_c$) as the first wave functions (eq. (87)) and a simple polynomial form of

$$\varphi_{nl}^{2\zeta}(r) = r^l(a_l - b_l r^2) \tag{88}$$

between the nucleus and the pre-defined split radius r_s [38]. In equation (88), the parameters a_l and b_l are chosen so that the function and its derivative are continuous at r_s.

2.3.6 Finite difference method

I ran the molecular dynamics calculations using the LCAO method in PAW, but some energetics calculations were performed using a method called finite difference method (FD), which is considered more accurate in energy calculations compared to the LCAO method [37]. In the finite difference method, the wave functions are calculated in the real-space grid so that the integrals over the space are changed to sums over the evenly-spaced grid points of the calculation box [14]. To enhance the results further, PAW method uses the double grid technique where an interpolation operator is used to interpolate the grid to even finer grid that consists of

2–5 times more points than the coarse grid [14]. Some local functions, including the smoothened frozen core electron density, the projector functions and the core potential (that makes the core states smooth but does not affect total energy [35]) are interpolated to the fine grid and are used to calculate the wave functions and energies in the coarse grid.

Because also the FD method requires an initial guess for the wave functions and electron density, in GPAW the first step of the SCF-cycle is calculated via LCAO method, after which the cycle is proceeded with FD.

2.4 Optimization: BFGS line search method

In chapter 2.2.4, the Kohn-Sham method was introduced with which the energies of the system with fixed atom positions are calculated. However, usually the initial positions of the atoms are not in the most stable state, but by moving the atoms one can minimize the potential energy of the system, that is one can optimize the structure. In our calculations this was done for some alkylthiols and thiol-gold structures to determine their stable states and the corresponding energies using Broyden–Fletcher–Goldfarb–Shanno (BFGS) line search method.

The BFGS algorithm is a general nonlinear optimization method for multiple variables [41], and in our case it is used to calculate the new positions of the nuclei after each SCF-cycle to get closer to the minimum potential energy of the system. Initially, the algorithm is given a convergence criterion for the maximum force in the system. After the first SCF-cycle, the forces are calculated for each atom. If the maximum force is greater than the set criterion, the atoms will be moved. First, the search direction p is calculated as

$$p = -\mathcal{H}F, \tag{89}$$

where $\mathcal{H}$ is a Hessian matrix, which at this point is a unit matrix, and F is the force matrix. The search step length matrix α is then determined via the line

search method where the Wolfe conditions

$$E(x + \alpha p) \leq E(x) + c_1 \alpha [F(x)]^T p \quad \text{and} \tag{90}$$

$$[F(x + \alpha p)]^T p \geq c_2 [F(x)]^T p \tag{91}$$

must meet [41]. In equations (90) and (91), E is the energy of the system, x is the position matrix of the system and c_1 and c_2 are optimization parameters which have $0 < c_1 < c_2 < 1$. In my calculations, they were set $c_1 = 0.23$ and $c_2 = 0.46$ (these are the default parameters in GPAW). After α is determined, the atoms are moved as $x \leftarrow x + \alpha p$, the new force matrix is calculated based on these atom positions (using the DFT machinery) and the procedure is replayed. Also, the Hessian matrix is recalculated for the next cycle via equation

$$\tilde{H} = (I - \frac{sy^T}{y^T s}) H (I - \frac{ys^T}{y^T s}) + \frac{ss^T}{y^T s}, \tag{92}$$

where I is a unit matrix and s and y have $s = \tilde{x} - x$ and $y = \tilde{F} - F$. The quantities with tilde denote the new value of a quantity.

When the cycle stops, *ie.* when the maximum force for an atom is smaller than the criterion value, the system is in relaxed state. The method does not necessarily find the global minimum for the energy of the structure but the inital positions of the atoms affect a lot to the final positions while using this method.

2.5 Molecular dynamics: Langevin thermostat

While BFGS line search method was implemented to relax structures to investigate their stable states and energies, the molecular dynamics simulations require a different approach to simulate the movement of atoms considering their thermal movement. There are many ways to simulate those quantities, and in my calculations I used the Langevin dynamics. In that method, every atom is given a random contribution to the force exerted to them, in addition to a certain friction coefficient that corresponds to damping of the atomic vibrations. The target is to set the system temperature to a certain value (that is calculated from the average

kinetic energy of the system), and so the method tries to simulate the chaotic behaviour of a heated atomistic system. The Langevin equation is basically the Newton's second law of the general form [42]

$$M\frac{\mathrm{d}^2X(t)}{\mathrm{d}t^2} = -\nabla E(X(t)) - \gamma M\frac{\mathrm{d}X(t)}{\mathrm{d}t} + R(t), \tag{93}$$

where M is the mass matrix that contains the masses of the atoms in the system, $X(t)$ is the position matrix of the nuclei as a function of time, γ is a pre-defined friction (or damping) factor and $R(t)$ is the random force matrix. The distibution of the random force R is related to the friction γ and the target temperature T as

$$\langle R(t)R(t')^\dagger\rangle = 2\gamma k_B T M\delta(t-t'). \tag{94}$$

Also, for the stationarity of the system, we require that $\langle R(t)\rangle = 0$.

In the DFT calculations, after the SCF-cycle has ended and the wave functions and the density corresponding to the present atom positions are found, the equation (93) is used to calculate the change of position for each atom. In the calculations, the Langevin equation (eq. (93)) has the form

$$F = Ma = -F_0 - \gamma p_0 + R, \tag{95}$$

where a is the acceleration matrix of the atoms and F_0 and p_0 are the initial forces and momenta of atoms. The new positions of the atoms, X_{new}, are then calculated via the Taylor series of the position as

$$X_{new} = X_0 + \Delta t\frac{\mathrm{d}X(t)}{\mathrm{d}t} + \frac{1}{2}(\Delta t)^2\frac{\mathrm{d}^2X(t)}{\mathrm{d}t^2} + \frac{1}{6}(\Delta t)^3\frac{\mathrm{d}^3X(t)}{\mathrm{d}t^3} + \dots \tag{96}$$

where the derivatives $\frac{\mathrm{d}X(t)}{\mathrm{d}t}$ and $\frac{\mathrm{d}^2X(t)}{\mathrm{d}t^2}$ have

$$\frac{\mathrm{d}X(t)}{\mathrm{d}t} = \frac{p_0}{M} \quad \text{and} \tag{97}$$

$$\frac{\mathrm{d}^2X(t)}{\mathrm{d}t^2} = \frac{F}{M}. \tag{98}$$

That is, the momentum has its old one at this stage, but the force on an atom is

taken as the newly calculated one. After the new positions are determined, the new momentum is also given by the Taylor series

$$p_{new} = p_0 + \Delta t \frac{\mathrm{d}p_0}{\mathrm{d}t} + \frac{1}{2}(\Delta t)^2 \frac{\mathrm{d}^2 p_0}{\mathrm{d}t^2} + \dots \tag{99}$$

After the positions, momenta and forces are calculated, a new SCF-calculation is set up and run. This procedure is then continued as long as it is necessary to simulate the phenomenon under investigation.

3 Results and discussion

In the calculations, the PBE functional was used throughout the work. The structure optimization was performed using the BFGS line search method, and Langevin dynamics algorithm was used in the molecular dynamics (MD) calculations. In the GPAW parameters, grid point spacing was 0.2 Å and Fermi width of 0.05 eV was used to smooth the orbital occupations. In all the calculations, there was 6–8 Å of vacuum between the unit cell boundaries and the nearest atom to let the wave functions behave naturally outside the molecules.

3.1 Energetic examination of thiols and gold structures

Before diving into the world of molecular dynamics simulations, let us make sure that my methods and systems under investigation are justified by determining the performance of the LCAO method, the energetics of the chemical reactions and the stability of the SAM structures. In this section, the energy differences in the reactions of the form

$$A \quad + \quad B \quad \rightarrow \quad C \quad + \quad D \tag{100}$$

are calculated as

$$\Delta E = [E(C) + E(D)] - [E(A) + E(B)] \tag{101}$$

where A, B, C and D are chemical compounds and $E(A)$ etc. are the corresponding energies. The energies are always the outputs of GPAW calculations, that is the energy difference between the structure and a non spin-polarized hydrogen atom; thus, their absolute values do not have much to analyze, but their differences are relevant as in equation (101). They usually have negative values, indicating that energy is released in the molecule-forming reaction and the structure is finally more stable than the initial state, *ie.* free atoms.

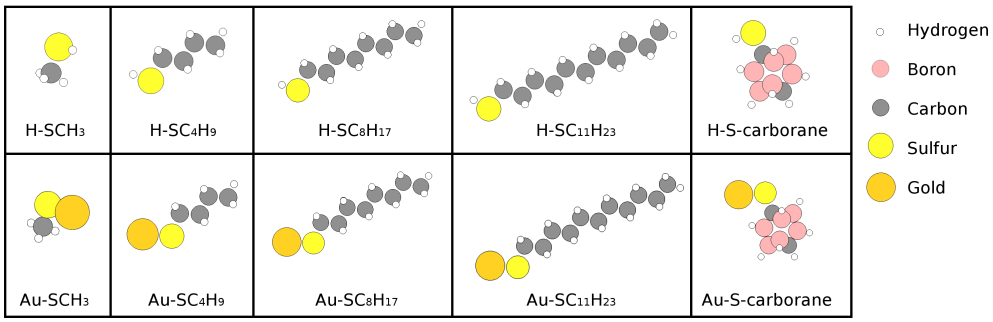

Figure 3: Molecular structures of different alkylthiols that were studied. The structures in the figure are the relaxed states from my optimization calculations.

3.1.1 Energetics of alkanethiols

Knowing that the finite difference method generally gives more accurate results than the LCAO approach, I ensured that the LCAO is usable in the molecular dynamics calculations because it is computationally more efficient than the FD method. I optimized the geometries of some simple alkylthiols (fig. 3) to compare the results between FD and LCAO calculations. In addition to alkanethiols, two more complex compounds were also investigated, namely H-S-carborane and Au-S-carborane. The carborane cluster consists of ten boron atoms and two carbon atoms that form an icosahedral cage (with a little distorted shape because of unsymmetric vertices) which can appear in meta- and para-isomers, depending on the mutual positions of the carbon atoms. In this study, the carborane had para-isomeric symmetry as shown in figure 3. The results including some specific bond lengths and bond angles are represented in tables 1 and 2, respectively.

First of all, the results show that my calculations match quite well with the literature values, the error being at most 2 percents (LCAO calculation of Au-S bond length in Au-SCH_3 molecule compared to the PBE value of Grönbeck [44]). While comparing the accuracy of FD and LCAO methods by relating them to the literature values, one can not, in fact, say if one performs better than the other. They have mutual difference both in bond lengths and angles but neither deviates significantly from the literature values, although my finite-difference results are closer to Grönbeck's computational values (ref. [44]). The biggest difference between

Table 1: Calculated bond lengths L in Ångstroms for simple alkanethiols together with literature values (when available). My results were calculated using both finite-difference method and LCAO method. The literature value for length of S-Au bonds in parenthesis that reappears in every gold compound is given in reference [43] for general alkyl group R in Au-SR molecules.

Molecule	Bond	L_{FD} [Å]	L_{LCAO} [Å]	$L_{Literature}$ [Å]
H-SCH_3	S-C	1.824	1.823	1.819 [43]
	S-H	1.354	1.370	1.35 [44], 1.34 [43]
Au-SCH_3	S-C	1.821	1.820	1.82 [44]
	S-Au	2.248	2.287	2.24 [44] (2.293 [43])
H-SC_4H_9	S-C	1.836	1.833	-
	S-H	1.353	1.369	-
Au-SC_4H_9	S-C	1.837	1.834	-
	S-Au	2.249	2.284	(2.293 [43])
H-SC_8H_{17}	S-C	1.835	1.837	-
	S-H	1.352	1.369	-
Au-SC_8H_{17}	S-C	1.840	1.838	-
	S-Au	2.247	2.281	(2.293 [43])
H-$SC_{11}H_{23}$	S-C	1.834	1.836	-
	S-H	1.353	1.371	-
Au-$SC_{11}H_{23}$	S-C	1.839	1.836	-
	S-Au	2.244	2.284	(2.293 [43])
H-S-carborane	S-C	1.805	1.808	-
	S-H	1.352	1.370	-
Au-S-carborane	S-C	1.807	1.809	-
	S-Au	2.252	2.286	(2.293 [43])

the results are in the cases of complexes that contain gold; the LCAO calculations produce systematically larger bond lengths between sulfur and gold and smaller Au-S-C bond angles. The difference can be accounted to the different ways of the methods to handle the wave functions that determine bonds between atoms, and it may cause different phenomena in the molecular dynamics simulations as these methods are repeated there thousands of times during a dynamics simulation. Due to my limited resources, however, only LCAO method was used in the simulations to perform faster calculations compared to the finite-difference method.

Optimizing the structures also gives the energies of the molecules. By calculating

Table 2: Calculated bond angles θ in degrees for simple alkanethiols together with literature values (when available). My results were calculated using both finite-difference method and LCAO method, and the PBE functional was used in both cases.

Molecule	Angle	θ_{FD} [°]	θ_{LCAO} [°]	$\theta_{\mathrm{literature}}$ [°]
H-SCH_3	H-S-C	96.5	96.3	96.5 [43]
	S-H-H	109.6	109.9	109.8 [43]
Au-SCH_3	Au-S-C	103.8	102.7	-
H-SC_4H_9	S-C-C	109.3	109.8	-
Au-SC_4H_9	Au-S-C	106.5	102.9	-
H-SC_8H_{17}	S-C-C	108.6	108.9	-
Au-SC_8H_{17}	Au-S-C	107.1	103.9	-
H-$SC_{11}H_{23}$	S-C-C	109.9	109.7	-
Au-$SC_{11}H_{23}$	Au-S-C	106.3	103.3	-
Au-S-carborane	Au-S-C	106.5	103.9	-

the energy change in the reaction

$$\cdot\mathrm{SR} \quad + \quad \mathrm{Au} \quad \rightarrow \quad \mathrm{AuSR}, \tag{102}$$

where R stands for the alkyl group, one can estimate the sulfur-gold bond stability. The energy values for different alkylthiols are shown in table 3. Firstly, the results show that the system state is (naturally) more stable in the right side of the reaction than in the left side, because the reaction energy change is negative. My results showed binding energies for Au-SR bond of about 3.0 eV and 2.3 eV for FD and LCAO calculations, respectively, while other GGA studies within DFT suggest the binding energy of 2.5 eV per molecule [45, 46]. Thus, based on my results, one can not say if one of the approaches, FD or LCAO, performs more accurately than the other.

Another thing that can be read from both the energy results and the geometry results, presented in this chapter, is that the length of the alkane chain does not seem to affect much to the properties of the S-Au bond. Also, the bond in question in the S-carborane structures seems to function in very similar way as in the alkane structures. This result suggests that while calculating the properties of structures consisting of thiols on top of gold surface, the alkyl chain does not affect the bonding between the sulfur end and the gold surface. However, the

Table 3: Calculated energy changes ΔE in electron volts in reactions of equation (102) where thiol radicals with different alkyl groups are bound to a gold atom. Both results of finite-difference (FD) and LCAO calculations are shown.

Molecule	ΔE_{FD} [eV]	ΔE_{LCAO} [eV]
SCH_3	-3.05	-2.28
SC_4H_9	-3.05	-2.30
SC_8H_{17}	-3.03	-2.29
$SC_{11}H_{23}$	-3.01	-2.30
S-carborane	-2.97	-2.28

alkyl composition probably affects the dynamics of the thiols during the removal (as the thiols interact with each other), but this effect is not investigated in this study.

3.1.2 Energetics of gold surface

The lattice constant of gold (fcc lattice) was optimized by calculating the energy of bulk gold with different lattice constants and checking which number gave the lowest energy; that energy and lattice constant correspond to the most stable structure. While the calculations were performed for periodic structures, it was necessary to calculate the quantities only for a unit cell of the structure. Namely, due to Bloch's theorem, the wave functions in infinite periodic structures can be written as $\psi_{\vec{k}}(\vec{r}) = e^{i\vec{k}\cdot\vec{r}}u(\vec{r})$ where $u(\vec{r})$ fulfils the same periodicity as the atomic structure [47]. This approach, however, requires the use of fine enough k-point grid, and for that purpose, I calculated the energy of a periodic structure (that was later used in nearly all calculations) as a function of k-point grid. The shape of the unit cell was 3x4 atoms in x and y directions, respectively, while the number of atoms in z-direction can be chosen arbitrarily for the k-point convergence calculations, because the lattice was chosen to be periodic only in x and y directions; the number of atoms in z-direction was chosen to be 1. The results of the k-point examination are shown in figure 4, which shows that the energy is converged enough for our needs at 4 or 5 k-points per direction. In the energy calculations presented in this study, both 4x4x1 and 5x5x1 k-point grids were used.

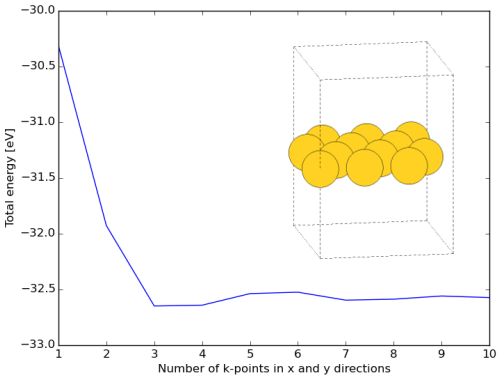

Figure 4: The total energy of Au unit cell, shown also in the figure, as a function of k-points in x and y directions. The unit cell consisted of 3x4x1 gold atoms in close-packed hexagonal lattice, periodic in the directions of the plane *ie.* in x and y directions.

All the results for gold lattices are collected in table 4. The calculation for the lattice constant gave 4.18 Å with 3x4 atoms unit cell and 5x5 k-point grid, while the experimental values for the lattice constant vary from 4.06 to 4.08 Å[48, 47]. The error is an acknowledged feature of the PBE functional, which often overestimates the lattice parameter compared to the experimental value [49]. Namely, other PBE studies have also received too large values, such as 4.154 Å[49] and 4.17 Å[44], meaning that my result is typical for the method in use. This calculation also gave the cohesion energy of gold, which is the average energy per atom needed to separate an infinite lattice to free atoms. The calculations gave the result of 3.21 eV per atom with 4x4x1 Monkhorst-Pack k-point grid and 3.19 eV per atom with 5x5x1 k-point grid using the finite difference method. The experimental value is 3.80 eV per atom [47], so my PBE calculations seem to underestimate the cohesion energy for gold. This is also a known result for PBE methods, as Jensen *et al.* reported of energy of 2.9 eV per atom [50] and Ferrighi *et al.* of energy of 3.02 eV per atom [51]. I also calculated the cohesion energy using the LCAO method, which gave 2.80 eV per atom, suggesting even poorer performance of the LCAO method in the energy calculations compared to the FD method.

In addition to bulk energies, the surface energy of Au(111) was calculated. The surface energy is the energy needed per atom to form a new surface from infinite

Table 4: Calculated quantities for gold lattice together with literature values. My results were calculated via finite-difference method and PBE functional.

Quantity	My result	Literature (PBE)	Literature (experimental)
Lattice constant [Å]	4.18	4.154 [49], 4.17 [44]	4.06 [48], 4.08 [47]
Cohesion energy [eV/atom]	3.2	2.9 [50], 3.02 [51]	3.80 [47]
Surface energy [J/m^2]	0.78	0.74 [52]	1.50 [53]

lattice. The equation

$$E_{\text{surf}} = 0.5 \times (E_u - N \times E_c)/n \tag{103}$$

was used, where E_u is the energy of the surface unit cell with N atoms and n surface atoms (periodic in the two directions of the plane) and E_c is the cohesion energy of gold. The result of calculations with 4x4x1 Monkhorst-Pack k-point lattice was 0.366 eV per surface atom or 0.775 J/m^2 in terms of the unit cell area, while another PBE study gave 0.35 eV per atom or 0.74 J/m^2 [52]. The experimental value for the surface energy is 1.50 J/m^2 [53], so the computational and experimental results do not match very well. It is noted, however, that the quantity is difficult to determine experimentally and the possibility of error is significant [52]. It is clear, however, that my results match with the other computational studies.

3.1.3 Energetics of alkanethiols on Au(111)

To make sure that the molecular dynamics simulations of thiols on gold surface are justified, I examined the energetics of some simple structures of that kind.

Adsorption energies were calculated for two kinds of processes: for a process where a single thiol is adsorbed on bridge site of the Au(111) surface, and for a process where an RS-Au-SR unit is formed on top of Au(111). However, different initial structures of thiols were considered, but only clean Au(111) surfaces were dealt with, *ie.* surfaces with no defects. The reactions and the corresponding changes in potential energy are presented in table 5.

The adsorption and binding energies are similar to the literature values, and the slight differences are assumed to be due to the computational methods. Namely,

Table 5: Calculated energy changes per thiol in the adsorption reactions together with literature values when available. The notation Au(s) indicates the gold surface Au(111) on which the thiols are adsorbed. The energy differences ΔE are calculated as the difference between the total potential energies of the right hand side and the left hand side of the equation. The finite-difference method was used in my calculations.

Reaction equation	ΔE [eV]	$\Delta E_{\text{literature}}$ [eV]
2 H-SCH_3 + Au(s) $\rightarrow$ H_2 + 2 H_3CS-Au(s)	-0.14	-
$\cdot SCH_3$ + Au(s) $\rightarrow$ H_3CS-Au(s)	-2.00	-1.95 [54, 55]
2 H-SCH_3 + Au(s) + Au $\rightarrow$ H_2 + H_3CS-Au-SCH_3-Au(s)	-0.63	-0.67 [51]
2 H-SC_4H_9 + Au(s) + Au $\rightarrow$ H_2 + H_9C_4S-Au-SC_4H_9-Au(s)	-0.71	-0.71 [51]
2 H-SC_8H_{17} + Au(s) $\rightarrow$ H_2 + 2 $H_{17}C_8$S-Au(s)	-0.14	-0.19 [56]
$\cdot SC_8H_{17}$ + Au(s) $\rightarrow$ $H_{17}C_8$S-Au(s)	-2.00	-

it was noticed during the calculations that even the grid point division affects the energies unexpectedly much. Thus, in systems of this size scale, the error in, for example, dissociative adsorption energy of H-SC_8H_{17} is not significant. The results show also that the binding energy of methanethiol and octanethiol are practically the same, meaning that the length of the alkane chain seems not to affect the Au-S bond strength of the thiol on Au(111) surface.

It is also notable that the binding energies of the thiols are of the order of 2 electron volts, while the energy to remove a gold atom from the surface has been determined to be between 0.7–1.0 eV ([57, 58, 59, 60, 61]). As was also seen from the alkanethiol calculations, the gold-sulfur bond in Au-SR molecule is larger than the surface energy. Therefore, one could expect that when pulling the thiol off from the surface, the bond that eventually breaks is not the bond between sulfur and gold but the bond between gold atoms. This conclusion is not strong, however, as the energy calculations do not give information about the binding mechanisms and the dynamics of the system, but only considers the initial and final states. Moreover, it was seen from the binding energies of the SC_8H_{17} thiol on different

Table 6: Binding energies of SC_8H_{17} adsorbed at different positions of Au(111) surface. The values are calculated according to the last equation of table 5.

Position	Binding energy [eV]
Bridge	-1.88
FCC	-1.91
A-top	-1.60
Bridge-HCP	-2.00

sites on Au(111) (table 6) that although the position between the bridge and hcp sites is the most stable one, the the binding energy at the a-top site (1.60 eV) is also larger than the surface energy of gold. Thus, while detaching thiols from the gold surface, the bond-breaking process should not be dependent on the adsorption site of the thiol.

3.2 Molecular dynamics

In all the molecular dynamics calculations, the system was first heated to 300 K using the Langevin dynamics with no constrains in the system. As the thiols were started to pull apart from gold, the dynamics were also continued using the Langevin dynamics. There are also methods available in which the system's kinetic energy is conserved such as Verlet's method [62], but now as the kinetic energy of the system is manipulated, it is better to use the Langevin method that describes the energetics of the dynamics in more realistic manner; the system can be considered to lie in heat bath of 300 K. Moreover, in the MD calculations, the mass of hydrogen atoms was increased to 2 atomic units, corresponding to deuterium; this was done for the efficiency of calculations, because the 2 fs time step that was used was too large for hydrogen atoms. Otherwise they could have run away from the system while having too great velocity given by the Langevin dynamics. This was assumed not to affect the dynamics of sulfur and gold that was the main point of interest in this study. The LCAO method was used in all molecular dynamics calculations.

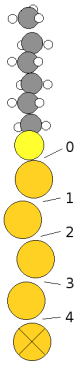

Figure 5: The initial structure of the test system which is investigated in chapter 3.2.1. The numbers denote the indices of the bonds between gold atoms in the chain.

3.2.1 Parameter tests in simple model system $Au_5SC_6H_{13}$

To investigate the effect of different computational parameters, I built a simple system which contained five gold atoms and a hexanethiol attached to the gold (figure 5). The tested parameters consisted of the Langevin friction parameter, pulling speed and the simulated temperature, which is also an input parameter to the Langevin thermostat calculator. The point of interest was that which bond breaks in the gold chain as the thiol is pulled off the system. In the test simulations, I constrained one of the gold atoms and pulled the thiol at constant velocity, that is, constrained the momentum of the furthest carbon atom of the thiol. The results in table 7 show the bonds which are broken in the simulations with different parameters. However, no correlation between any parameter and the broken bond can be read from these results; there is no systematic change in the broken bond index as moving either to higher pulling speeds or to higher friction parameters. The doubling of the temperature results in the detaching of only one gold atom, but this amount of data is not sufficient to say anything with certainty. After all, the use of room temperature in the simulations is justified as the objective is to mimic the environment in the chemical lift-off lithography experiment [1].

To get a better view of the likelihood of the bond breaking, I examined two of the processes more carefully. In the figure 6 there is a plot of all the bond lengths in the gold atom chain of the test system (figure 5) as functions of the pulled distance. The lines show quite similar and reasonable features, but to better investigate the

Table 7: The bonds that were broken in the pulling simulation test, where the thiol was pulled apart from a gold chain of 5 atoms. The quantites have v for pulling velocity, T for temperature and γ for the Langevin friction parameter. The bond indeces correspond to the bonds in figure 5. In the case of "3,1" bond index the pulling velocity was so high that the chain was broken in two places, at bonds 3 and 1.

v [Å/ps]	T [K]	γ [fs^{-1}]	Broken bond index
0.1	300	0.004	3
0.5	300	0.001	3
		0.004	3
		0.010	1
		0.020	3
		0.040	1
1.0	300	0.004	3
		0.020	2
2.5	300	0.004	1,3
		0.020	3
0.5	600	0.004	1
		0.040	1

oscillation of the atoms, the standard deviations of the oscillations were calculated for two ranges: the whole oscillation part before the bond breaking (up to 5.8 Å pulling distance) and the part near the bond breaking (from 4.3 Å to 5.8 Å). The results are in table 8. Firstly, the oscillations seem to be more intense in the calculations with the smaller friction parameter, which was expected as the amount of friction tells how much the movement is being disturbed. Secondly, the oscillations near the bond breaking are smaller than the overall oscillation, which can be explained by the shape of the chain: when the chain is nearly straight near the bond breaking, the atoms are more constrained and not so free to oscillate. It is also seen that the bond 3 has systematically the largest deviations, indicating more intense oscillation, and the bond 1 has the next largest deviation at least in the near-breaking oscillations. The bonds 1 and 3 are also the most abundant in table 7, suggesting that there is some correlation between the freedom of movement and the likelihood of the bond breaking. However, the bond 3 oscillates more than bond 1 in the 0.040 fs^{-1} friction parameter calculation, but still the bond 1 is broken, implying that the oscillation does not tell the whole truth. Namely, it has to be

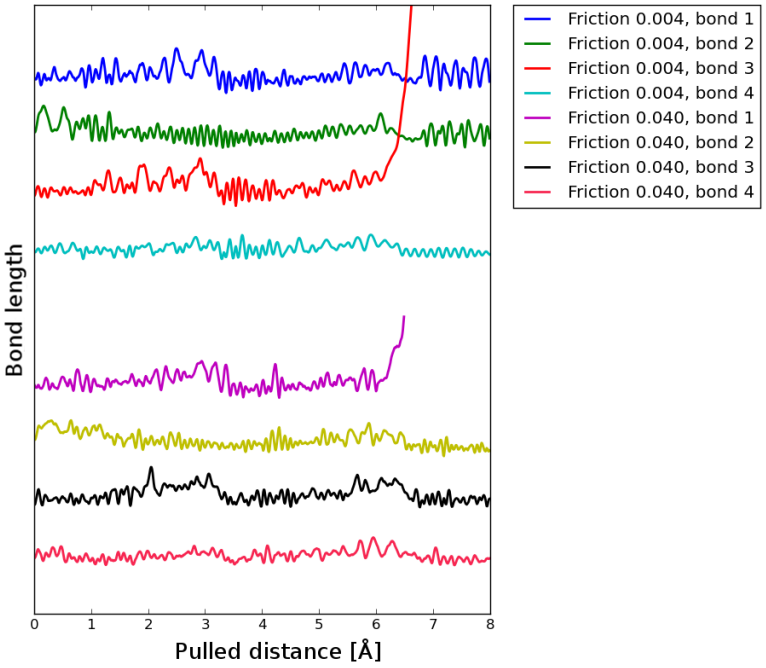

(a) (b)

Figure 6: The bond lengths in the pulling processes of the $Au_5SC_6H_{13}$ test system. (a) The four upper lines correspond to a calculation with pulling speed 0.5 Å/fs and friction parameter of 0.004 fs^{-1} and the lower four to the same system with friction parameter 0.040 fs^{-1}. The x-axis tells how much the terminal carbon of the thiol molecule has been moved. The lines having the same friction parameter have been offset 1 Å from each other and the 0.004 fs^{-1} friction parameter lines have been offset 2.5 Å above the higher friction parameter lines for clarity. The rising ends of the third and fifth lines indicate the broken bonds and their end features have been cut off in the figure for clarity. (b) The initial structure of the calculations.

noted that the oscillation and bond breaking are both probably consequence of some other feature of the system (most probably the shape of the wave functions), meaning that the oscillation itself does not determine the bond that breaks.

Going even further with this test system, I also calculated the energies and forces at different steps of the pulling process, and did this by forcing the bond breakage at different parts of the chain. The thiol and the gold atoms that were wanted to stay with the thiol were moved 0.2 Å at a time, and the system was relaxed after moving the atoms. The terminal carbon atom was also constrained together

Table 8: The standard deviations in oscillations shown in figure 6. The column $\delta L_{0.0,5.8}$ gives the standard deviations of the whole oscillation parts before the bond breaking (up to 5.8 Å deviation) and the column $\delta L_{4.3,5.8}$ gives the part near the bond breaking (from 4.3 Å to 5.8 Å). Also, the broken bonds in different calculations are marked in the table.

Friction parameter	Bond index	$\delta L_{0.0,5.8}$ [Å]	$\delta L_{4.3,5.8}$ [Å]	
0.004	1	0.141	0.097	
	2	0.140	0.079	
	3	0.151	0.105	(broken bond)
	4	0.082	0.079	
0.040	1	0.129	0.091	(broken bond)
	2	0.129	0.090	
	3	0.129	0.101	
	4	0.076	0.073	

with the one gold atom to prevent the system from recombining, and the distance between the atoms whose bond was wanted to break was constrained (after moving the atoms) in order to break exactly that bond.

The resulting energies and forces in relaxed states as functions of the pulled distances are plotted in the figure 7 (the forces were calculated after removing the constraints from the system). From figure 7a it can be seen that the energy of the system satures to a certain energy as the thiol is pulled far enough from the gold system, but the energies are different for different systems. This tells that the chain is easiest to separate by breaking the bond number 3 (in notation of figure 5), which has the lowest saturation energy; 0.1 eV above it there lies the energy of the process where only one atom is detached from the chain. The other options are less likely, which was also seen in the parameter tests, table 7: mostly bonds with indeces 1 and 3 were broken. It is notable that the order of the energy lines is the same over the whole pulled-distance range, indicating that the whole process favours breaking the bond 3. This is also seen in the force figure (fig. 7b) where, for all the systems, there are peaks somewhere between 0.4 Å and 0.8 Å in pulling distance, where the bond breaking essentially occurs. The maxima of these peaks can be considered as threshold forces that has to be exerted to the atom for the bond to break. It can be seen that the order of the thresholds for different bonds correspond perfectly to the order shown by the energy lines.

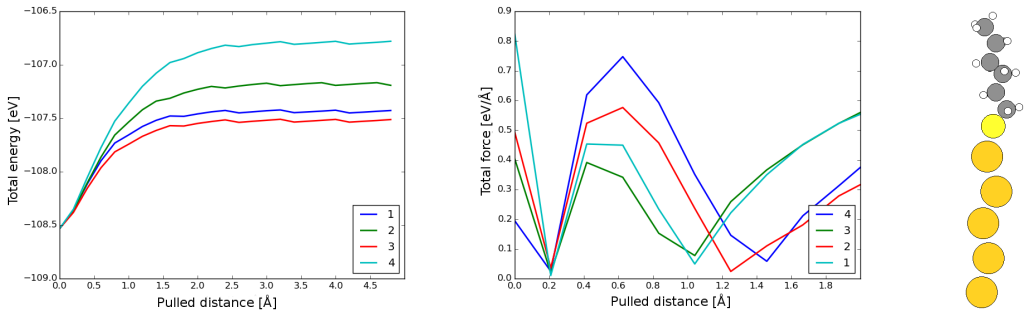

(a) (b) (c)

Figure 7: Energy and forces of the $Au_5SC_6H_{13}$ system versus the pulled distance of the thiol. Each plotted line corresponds to a single simulation where a certain Au-Au bond of the model system is broken. The labels of the plot lines correspond to the broken bond indices. (a) The energies are the total energies of the systems. (b) The forces are calculated for the last gold atom that is detached from the rest of the gold and transferred to the thiol-gold complex. (c) The initial structure of the calculations.

My calculations have thus shown in three different ways that the thiol-pulling process for the test system results most likely in the bond breaking at bond 3. The result is not quite intuitive, as one would expect that two gold atoms would be more likely to break from the chain than three atoms, but apparently the electronic wave functions behave in such a way that the third bond is the least stable. Kruger et al. [63] also performed calculations were they pulled a single thiol off from Au(221) surface, and they also ended up with removal of three gold atoms with the ethylthiol. Thus, my results fit well to their findings. Also, while the energy difference between the bond breaking at indices 1 and 3 was small, the pulling result in more complex systems (such as the ones respresented in the next chapter) may not be predictable, as there can be factors in the complex structure that disturb the pulling process. Already the average kinetic energy of the particles is about 0.04 eV in the temperature of 300 K, meaning that there is also some unpredictability in the result of the pulling process, mostly related to the interactions between gold atoms.

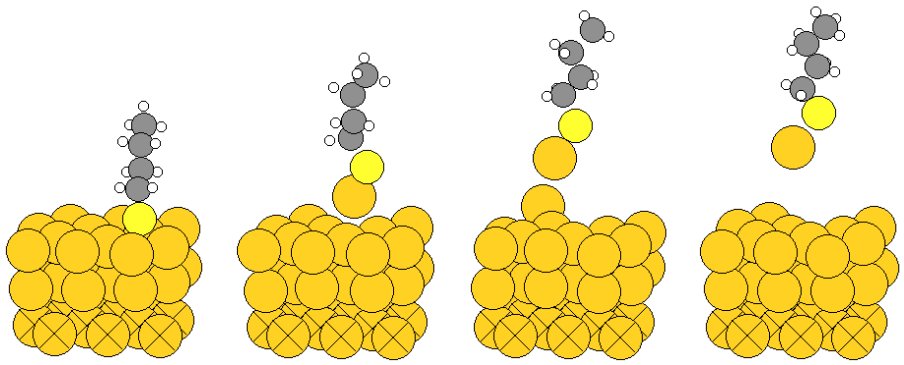

Figure 8: The critical stages when pulling the low-coverage thiols off from the Au(111) surface. There is only the unit cell shown in the figure which was set periodic in the directions of the surface.

3.2.2 Removing thiols from gold surface

Let us move on to the simulation systems with thiols adsorbed onto gold surface and then pulled off. First, low-coverage simulations were calculated, where only one thiol is attached to the unit cell of 3x4x3 gold atoms forming a Au(111) surface and then pulled off. The friction parameter here was 0.04 fs^{-1}. The most critical stages of the simulation are shown in figure 8, and it is seen that a gold atom bound to the sulfur is lifted off, leaving a vacancy to the (111)-surface. This was expected, based on the energy calculations in chapter 3.1. It can be seen that another gold atom is also nearly pulled off, but the interaction between that atom and the eventually-pulled-off atom is too weak overcome the force exerted by the surface to the other atom. Generally, the result is surprising in a sense that you can reconstruct surface made of gold, the most inert noble metal, by removing a simple thiol from it.

A couple of similar calculations were also run for an RS-Au-SR unit on the surface by pulling the carbon end of the other thiol. Calculations with no vacancies and with one and two vacancies per unit cell were run, but in all those simulations no extra gold was pulled off but only the RS-Au-SR unit was removed as a whole. This kind of system is assumed to form for simple thiols while the SAM is fabricated

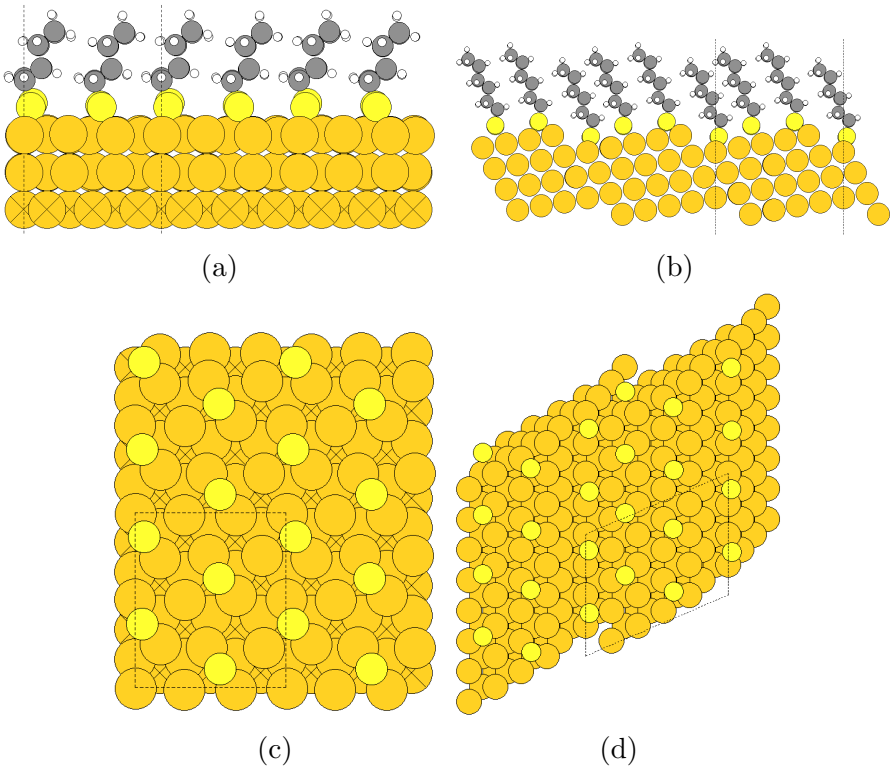

Figure 9: Calculated systems with high-coverage of thiols on Au(111) and Au(332) surfaces. The dashed lines indicate the boundaries of the unit cells. (a) Pure Au(111) surface with full coverage of butanethiols SC_4H_9. There are three unit cells shown. (b) Pure Au(332) surface with full coverage of hexanethiols SC_6H_{13}. There are three unit cells shown. (c) and (d) Same as figures a and b, respectively, but shown from the top of the surface and with 2x2 unit cells. The alkane chains have been removed to illustrate the initial positions of the sulfur atoms on the surface.

[20], and recalling that Liao *et al.* reported that a single layer of gold was removed in the SAM pulling process [1], this result does not fit to those observations and assumptions of the RS-Au-SR unit structure observations.

Getting further, what if there were more than one thiol on the surface and they all got ripped off at the same time, leaving multiple vacancies on the surface and thus greatly reducing the surface energy? I calculated that kind of simulations for two kinds of systems with two different Langevin friction parameters. In these simulations, k-point grid of 2x2x1 was used for 3x4x3 Au(111) surface unit cell and only gamma k-points for the Au(332) surface unit cell, shown in figure 9. The

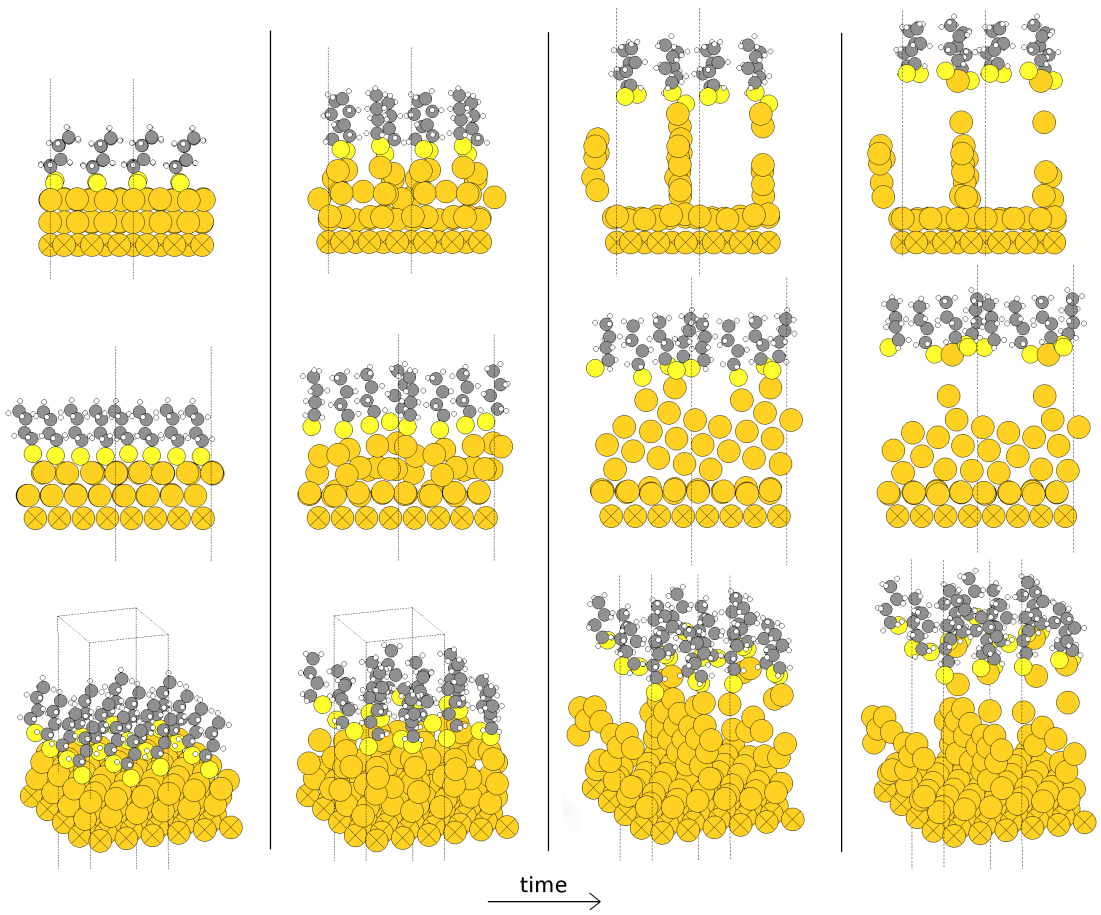

Figure 10: Some steps of pulling high-coverage thiol monolayers from Au(111) with Langevin friction parameter 0.04 fs^{-1}. There are four time steps at which the structure is shown from different points of view, and the process is going forwards to the right. In each subfigure, there are 2x2 unit cells side by side.

error of the coarser k-point grids is not assumed to be significant in this qualitative examination. The pulling velocity was 0.5 Å per picosecond, and the simulated temperature was 300 K. Two different Langevin friction parameters were used (0.04 fs^{-1} and 0.002 fs^{-1}), resulting in remarkably different phenomena during the pulling processes, as shall be seen.

Let us first look at the process for full coverage ($2\sqrt{3} \times \sqrt{3}$ adsorption structure) of butylthiols on Au(111) surface. The critical stages of calculation with the friction parameter 0.04 fs^{-1} are shown in figure 10. The simulation shows a very interesting

phenomenon, where the top layer of gold is reconstructed to the shape of a wall on top of the other gold layers as the thiol cover is lifted. This wall is eventually detached from the thiols and left on the surface, while one gold atom is left with the thiols, forming a RS-Au-SR unit when separated from the surface. The two other thiols in the unit cell formed a dithiol unit and, in the end, pulled no gold along.

The friction parameter was then decreased to 0.002 fs^{-1} and the simulation was repeated. The results of this calculation are shown in figure 11. There is also some minor wall-forming in this case but not so clearly as in the simulation with higher friction parameter. What is notable here, however, is that remarkably more gold

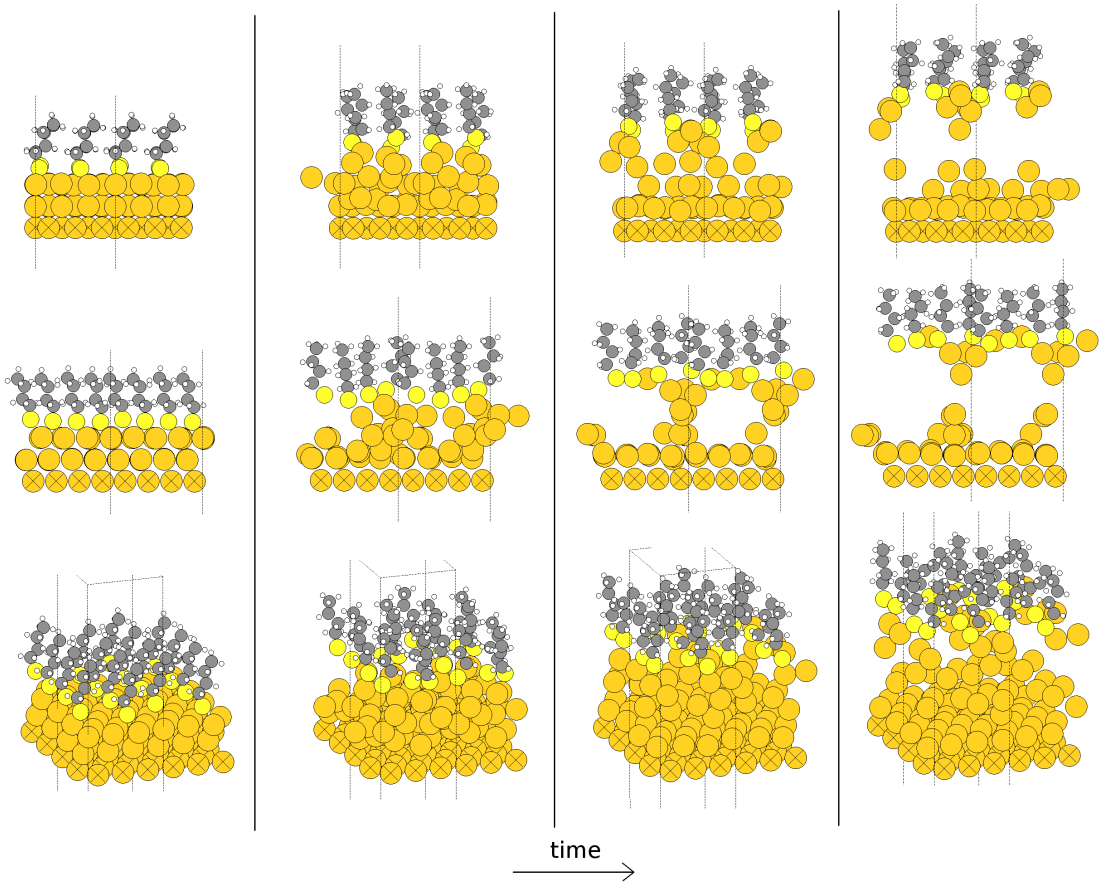

Figure 11: Some steps of pulling high-coverage thiol monolayers from Au(111) with Langevin friction parameter 0.002 fs^{-1}. There are four time steps at which the structure is shown from different points of view, and the process is going forwards to the right.

is detached from the surface. Actually, half of the top gold layer is removed with the thiols in the lifting process. This suggests that the friction parameter has an unexpectedly large effect in the dynamics of gold (it is the gold-gold bonds that seem to behave differently in these two simulations).

Indeed, the same phenomenon is observed when calculating the dynamics in the case of Au(332) surface, from which a dense cover of SC_6H_{13} thiols was pulled off. The process with friction parameter 0.04 fs^{-1} is shown in figure 12 and the one with parameter 0.002 fs^{-1} in figure 13. In both cases, a gold chain is formed between the pulled thiols and the gold surface and the chain is broken at some point. But in the big picture, it happens again that smaller friction parameter

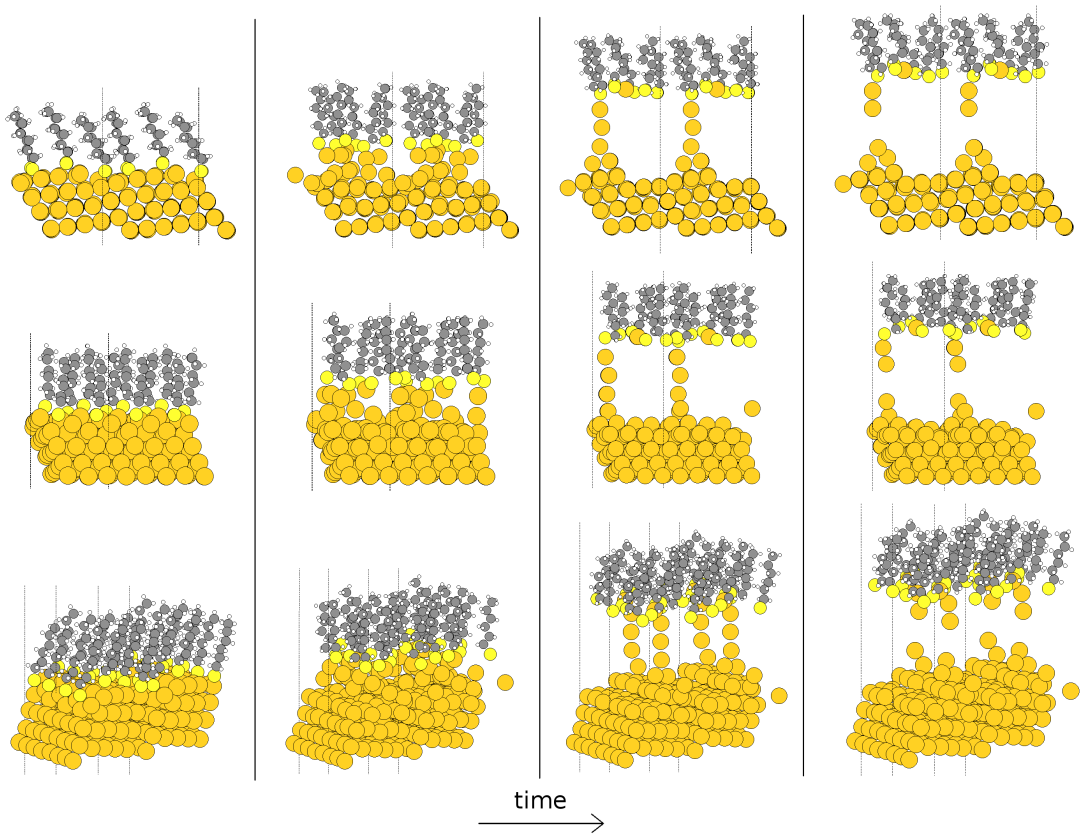

Figure 12: Some steps of pulling high-coverage thiol monolayers from Au(332) with Langevin friction parameter 0.02 fs^{-1}. There are four time steps at which the structure is shown from different points of view, and the process is going forwards to the right.

leads to bigger yield in pulled-off gold atoms, as 3 gold atoms per unit cell are pulled off with the larger parameter and 6 atoms per unit cell with the smaller parameter.

What is also seen from all these high-coverage simulations is that RS-Au-SR units between two thiols are quickly formed when the pulling process is started, and in the case of the higher friction parameter, some thiols bind to each other forming dithiols. The problem with the pulling processes with large friction parameter seems to be that these units have weaker tendency to pull more gold with themselves. Probably, the large friction parameter slows down the gold atoms too much, so that they have no time to react to the more rapid movement of the lighter atoms such as sulfur. Thus, it can be deduced that the smaller friction parameter gives

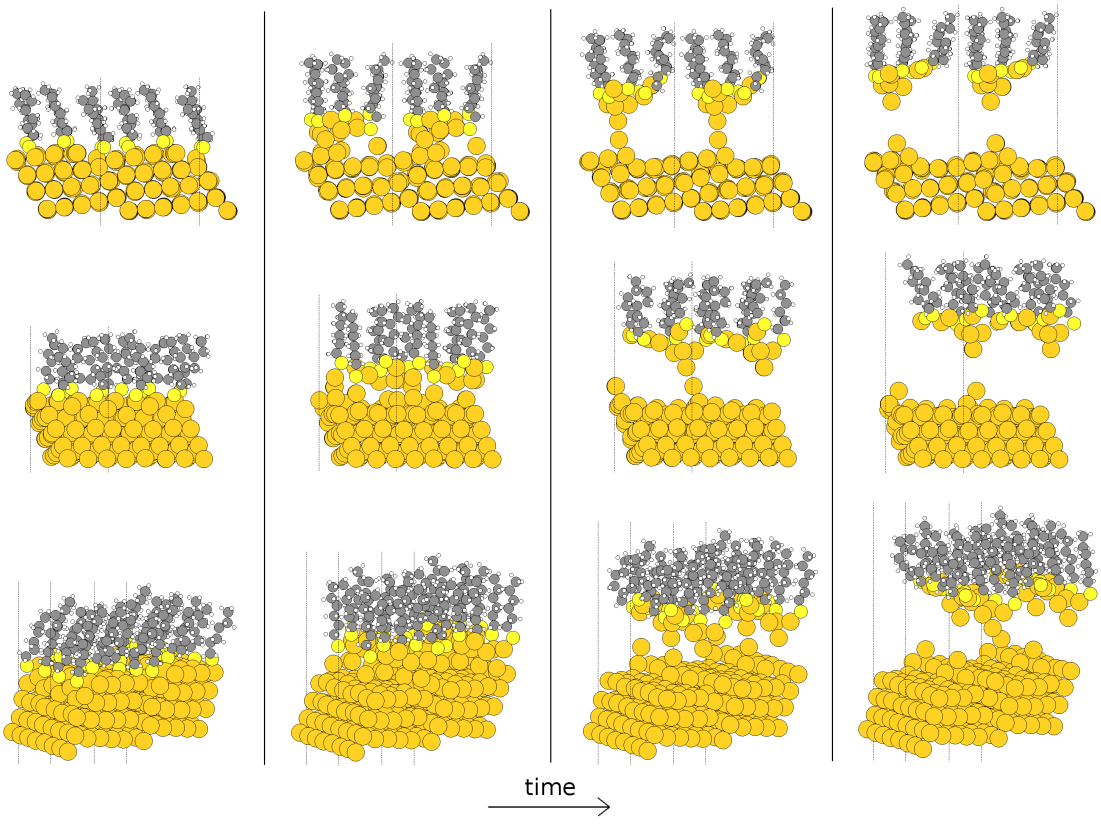

Figure 13: Some steps of pulling high-coverage thiol monolayers from Au(332) with Langevin friction parameter 0.004 fs^{-1}. There are four time steps at which the structure is shown from different points of view, and the process is going forwards to the right.

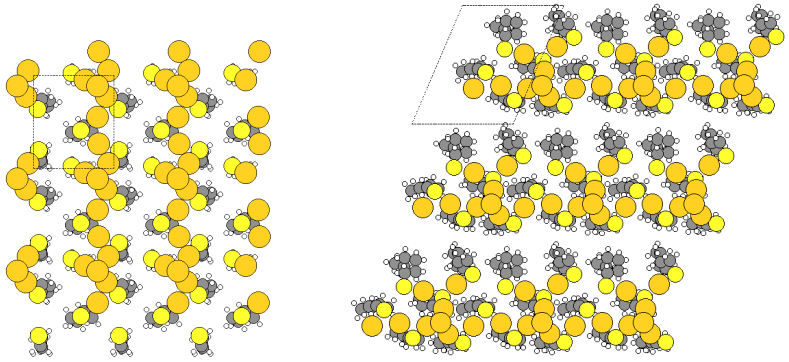

(a) (b)

Figure 14: The patterns of removed thiols and gold in the final frames of the 0.002 fs^{-1} friction parameter simulations. Figure (a) corresponds to the process represented in figure 11 and figure (b) corresponds to figure 13. The dashed lines are borders of the computational unit cells, so there are 3x3 unit cells in these figures.

more realistic results, as Liao *et al.* [1] observed that a single layer of gold is removed at the pulling process.

Let us then look at the outcome of these pulling processes. Namely, the resulting thiol-gold structures of the 0.002 fs^{-1} friction parameter calculations show interesting chain-like patterns, shown in figure 14, where there are -S-Au-S-Au- structures and also tetrahedral, 4-atom gold clusters in the chains. I also ran some simulations where these structures were let to evolve in time, but no significant change in the structure was observed. Therefore, the structures are quite stable already after the bonds to the surface have broken. However, the problem in analysing this pattern and its meaning is that the computational unit cells are quite small in a sense that the chains have no opportunity to show any superstructures or statistical probabilities in the gold-pyramid formation, for example. Still, it is interesting that both the simulations, for Au(111) and Au(332), result in nearly similar thiol-gold structures with the formation of the gold pyramids.

4 Conclusions

The goal of this study was to get closer to understanding the phenomena of processes where alkylthiol monolayers are removed from gold surfaces. Molecular dynamics simulations within density functional theory (DFT) were performed to investigate what happens at the interface of gold surface and thiols adsorbed onto it. Also, energetics calculations were run in order to get a clue of the nature of the gold-sulfur bond. The results of the energetics calculations were reasonable compared to each other and fit well to the literature values.

The main result of this study was that in the simulations of high-coverage thiol monolayers on Au(111) and Au(332) surfaces, using small enough Langevin friction parameter leads to removal of about half of the top layer of the gold surface. The experiment of Liao *et al.* [1] suggests that *"a single atomic layer is removed during the lift-off process"*. According to the numbers in the publication, the depth of the gold layer is changed 4 ± 3 Å during the lift-off, while the theoretical depth of a Au(111) layer is about 2.4 Å. Thus, it might be that the gold layer was not removed as a whole, or perhaps three layers were removed. Maybe gold was removed locally from some area and somewhere there were lots of adatoms; this is difficult to say without knowing the exact experimental setup, that is, if this study is comparable to their results. In any case, my calculations showed that gold surface can be reconstructed by lifting the thiol monolayer off the surface.

A lot remains to be calculated. For example, in my calculations only single thiols at the bridge sites of gold surface were investigated using the assumably more realistic Langevin friction parameter, while the more realistic system would perhaps contain vacancies and RS-Au-SR units. The thiolates with different alkyl chain, for example the carborane molecule, could also lead to different electron wave function behavior at the sulfur end. Moreover, the Bader charge analysis would also be fruitful in the binding analysis, as Xue *et al.* have only recently found that the strength of the gold-thiolate interaction could be increased by oxidizing the gold surface [64].

Also, it would be fruitful to repeat at least some of my calculations with more

accurate methods, for example by replacing the LCAO method with FD method in the dynamics calculations. The next step towards more accurate simulations would be to increase the k-point density. In addition, enlarging the unit cell would lead to larger variety of alternative phenomena in the simulations that could show the likelihood of different physical phenomena in the system, and therefore it could lead to more realistic simulations. Also the dispersive (van der Waals) forces were not taken into account in my calculations; they could affect the interaction between the thiolates in the SAM structures in such a way that the disulfur units would not form so easily. Moreover, in real systems, there are no such thing as pure Au(111) or Au(332) surface, but there are always some defects and differently formed structures in surfaces. This becomes a problem in all kinds of simulating as the number of ways to build the system to be simulated increases so that all the issues can not be processed. Also, while the system has some internal randomness, such as the uncertainty principle in real systems and the Langevin temperature in my calculations, one can never achieve a one-and-only result for systems this big. If the calculations were computationally less demanding, one could run the same calculation a few times and make statistics of the results and that way describe the different possibilities in the process. However, as in all computational science, more accurate methods need more computational resources which are always the limiting factor; otherwise everything would have already been calculated.

Anyhow, the objective of this study is fulfilled, as some basic information of the computational parameters needed for the simulated phenomenon was acquired. Also, the phenomena that were observed builds base for the theoretical research of the SAM lift-off process.

References

[1] W.-S. Liao, S. Cheunkar, H. H. Cao, H. R. Bednar, P. S. Weiss, and A. M. Andrews, "Subtractive patterning via chemical lift-off lithography.," *Science (New York, N.Y.)*, vol. 337, pp. 1517–21, Sept. 2012.

[2] D. Nuzzo, R.G.; Allara, R. G. Nuzzo, and D. L. Allara, "Adsorption of Bifunctional Disulfides on Gold Surfaces," *J. Am. Chem. Soc.*, vol. 105, pp. 4481–4483, 1983.

[3] J. C. Love, L. a. Estroff, J. K. Kriebel, R. G. Nuzzo, and G. M. Whitesides, "Self-assembled monolayers of thiolates on metals as a form of nanotechnology.," *Chemical reviews*, vol. 105, no. 4, pp. 1103–69, 2005.

[4] A. Ulman, "Formation and Structure of Self-Assembled Monolayers.," *Chemical Reviews*, vol. 96, pp. 1533–1554, 1996.

[5] D. G. Castner and B. D. Ratner, "Biomedical surface science: Foundations to frontiers," *Surface Science*, vol. 500, pp. 28–60, 2002.

[6] A. J. Haes and R. P. Van Duyne, "A Nanoscale Optical Biosensor: Sensitivity and Selectivity of an Approach Based on the Localized Surface Plasmon Resonance Spectroscopy of Triangular Silver Nanoparticles," *Journal of the American Chemical Society*, vol. 124, pp. 10596–10604, Sept. 2002.

[7] L. Srisombat, A. C. Jamison, and T. R. Lee, "Stability: A key issue for self-assembled monolayers on gold as thin-film coatings and nanoparticle protectants," *Colloids and Surfaces A: Physicochemical and Engineering Aspects*, vol. 390, pp. 1–19, Oct. 2011.

[8] M. C. Daniel and D. Astruc, "Gold Nanoparticles: Assembly, Supramolecular Chemistry, Quantum-Size-Related Properties, and Applications Toward Biology, Catalysis, and Nanotechnology," 2004.

[9] M. D. Malinsky, K. L. Kelly, G. C. Schatz, and R. P. Van Duyne, "Chain length dependence and sensing capabilities of the localized surface plasmon resonance of silver nanoparticles chemically modified with alkanethiol self-assembled monolayers," *Journal of the American Chemical Society*, vol. 123, pp. 1471–1482, 2001.

[10] R. Elghanian, J. J. Storhoff, R. C. Mucic, R. L. Letsinger, and C. A. Mirkin, "Selective colorimetric detection of polynucleotides based on the distance-dependent optical properties of gold nanoparticles.," *Science (New York, N.Y.)*, vol. 277, pp. 1078–1081, 1997.

[11] J. Liu and Y. Lu, "A colorimetric lead biosensor using DNAzyme-directed assembly of gold nanoparticles," *Journal of the American Chemical Society*, vol. 125, pp. 6642–6643, 2003.

[12] A. K. Salem, P. C. Searson, and K. W. Leong, "Multifunctional nanorods for gene delivery.," *Nature materials*, vol. 2, pp. 668–71, Oct. 2003.

[13] R. Singhvi, A. Kumar, G. Lopez, G. Stephanopoulos, D. Wang, G. Whitesides, and D. Ingber, "Engineering cell shape and function," *Science*, vol. 264, pp. 696–698, Apr. 1994.

[14] J. Mortensen, L. Hansen, and K. Jacobsen, "Real-space grid implementation of the projector augmented wave method," *Physical Review B*, vol. 71, p. 035109, Jan. 2005.

[15] J. Enkovaara, C. Rostgaard, J. J. Mortensen, J. Chen, M. Dułak, L. Ferrighi, J. Gavnholt, C. Glinsvad, V. Haikola, H. A. Hansen, H. H. Kristoffersen, M. Kuisma, A. H. Larsen, L. Lehtovaara, M. Ljungberg, O. Lopez-Acevedo, P. G. Moses, J. Ojanen, T. Olsen, V. Petzold, N. A. Romero, J. Stausholm-Mø ller, M. Strange, G. A. Tritsaris, M. Vanin, M. Walter, B. Hammer, H. Häkkinen, G. K. H. Madsen, R. M. Nieminen, J. K. Nø rskov, M. Puska, T. T. Rantala, J. Schiø tz, K. S. Thygesen, and K. W. Jacobsen, "Electronic structure calculations with GPAW: a real-space implementation of the projector augmented-wave method.," *Journal of physics. Condensed matter : an Institute of Physics journal*, vol. 22, p. 253202, June 2010.

[16] S. R. Bahn and K. W. Jacobsen, "An object-oriented scripting interface to a legacy electronic structure code," *Computing in Science and Engineering*, vol. 4, pp. 56–66, 2002.

[17] H. Häkkinen, "The gold-sulfur interface at the nanoscale.," *Nature chemistry*, vol. 4, pp. 443–55, June 2012.

[18] H. Grönbeck, M. Walter, and H. Häkkinen, "Theoretical characterization of cyclic thiolated gold clusters.," *Journal of the American Chemical Society*, vol. 128, pp. 10268–75, Aug. 2006.

[19] E. Pensa, E. Cortés, G. Corthey, P. Carro, C. Vericat, M. H. Fonticelli, G. Benítez, A. A. Rubert, and R. C. Salvarezza, "The chemistry of the sulfur-gold interface: In search of a unified model," *Accounts of Chemical Research*, vol. 45, pp. 1183–1192, 2012.

[20] P. Maksymovych, O. Voznyy, D. B. Dougherty, D. C. Sorescu, and J. T. Yates, "Gold adatom as a key structural component in self-assembled monolayers of organosulfur molecules on Au(111)," *Progress in Surface Science*, vol. 85, pp. 206–240, May 2010.

[21] T. Hayashi, Y. Morikawa, and H. Nozoye, "Adsorption state of dimethyl disulfide on Au(111): Evidence for adsorption as thiolate at the bridge site," *Journal of Chemical Physics*, vol. 114, pp. 7615–7621, 2001.

[22] Y. Yourdshahyan and A. M. Rappe, "Structure and energetics of alkanethiol adsorption on the Au(111) surface," *The Journal of Chemical Physics*, vol. 117, no. 2, p. 825, 2002.

[23] P. Maksymovych, D. C. Sorescu, and J. T. Yates, "Gold-adatom-mediated bonding in self-assembled short-chain alkanethiolate species on the Au(111) surface," *Physical Review Letters*, vol. 97, 2006.

[24] P. Hohenberg and W. Kohn, "Inhomogeneous electron gas," *Physical review*, vol. 136, pp. B864–B871, Nov. 1964.

[25] L. H. Thomas, "The calculation of atomic fields," *Mathematical Proceedings of the Cambridge Philosophical Society*, vol. 23, p. 542, Oct. 2008.

[26] R. G. Parr and W. Yang, *Density-Functional Theory of Atoms and Molecules*, vol. 16. International Journal of Quantum Chemistry, 1989.

[27] W. Koch and M. C. Holthausen, *A Chemist's Guide to Density Functional Theory*, vol. 3. Neural Networks, 2001.

[28] C. Roothaan, "New Developments in Molecular Orbital Theory," *Reviews of Modern Physics*, vol. 23, pp. 69–89, Apr. 1951.

[29] J. C. Slater, "The theory of complex spectra," *Physical Review*, vol. 34, pp. 1293–1322, 1929.

[30] W. Kohn and L. J. Sham, "Self-Consistent Equations Including Exchange and Correlation Effects," *Physical Review*, vol. 140, pp. A1133–A1138, Nov. 1965.

[31] P. A. M. Dirac, "Note on Exchange Phenomena in the Thomas Atom," *Mathematical Proceedings of the Cambridge Philosophical Society*, vol. 26, p. 376, Oct. 2008.

[32] J. P. Perdew and Y. Wang, "Accurate and simple analytic representation of the electron-gas correlation energy," *Physical Review B*, vol. 45, pp. 13244–13249, 1992.

[33] S. H. Vosko, L. Wilk, and M. Nusair, "Accurate spin-dependent electron liquid correlation energies for local spin density calculations: a critical analysis," *Canadian Journal of Physics*, vol. 58, pp. 1200–1211, Aug. 1980.

[34] J. P. Perdew, M. Ernzerhof, and K. Burke, "Generalized gradient approximation made simple," *Physical Review Letters*, vol. 77, pp. 3865–3868, 1996.

[35] P. E. Blöchl, "Projector augmented-wave method," *Physical Review B*, vol. 50, pp. 17953–17979, Dec. 1994.

[36] P. Schwerdtfeger, "The pseudopotential approximation in electronic structure theory.," *Chemphyschem : a European journal of chemical physics and physical chemistry*, vol. 12, pp. 3143–55, Dec. 2011.

[37] A. H. Larsen, M. Vanin, J. J. Mortensen, K. S. Thygesen, and K. W. Jacobsen, "Localized atomic basis set in the projector augmented wave method," *Physical Review B*, vol. 80, p. 195112, Nov. 2009.

[38] M. Soler, E. Artacho, J. D. Gale, A. Garc, J. Junquera, P. Ordej, and S. Daniel, "The SIESTA method for ab initio order- N materials," *J. Phys.: Condens. Matter*, vol. 14, pp. 2745–2779, 2002.

[39] O. F. Sankey and D. J. Niklewski, "Ab initio multicenter tight-binding model for molecular-dynamics simulations and other applications in covalent systems," *Physical Review B*, vol. 40, pp. 3979–3995, 1989.

[40] J. Junquera, O. Paz, D. Sánchez-Portal, and E. Artacho, "Numerical atomic orbitals for linear-scaling calculations," *Physical Review B*, vol. 64, p. 235111, Nov. 2001.

[41] J. Nocedal and S. J. Wright, *Numerical Optimization*, vol. 43. Springer, 1999.

[42] T. Schlick, *Molecular Modeling and Simulation*, vol. 21. Springer, 2002.

[43] E. David R Lide, "CRC Handbook of Chemistry and Physics, Internet Version 2005," *CRC Press, Taylor and Francis Boca Raton FL*, p. 0, 2005.

[44] H. Grönbeck, "Thiolate induced reconstruction of Au(111) and Cu(111) investigated by density functional theory calculations," in *Journal of Physical Chemistry C*, vol. 114, pp. 15973–15978, 2010.

[45] R. L. Johnston, "Metal nanoparticles and nanoalloys," *Frontiers of Nanoscience*, vol. 3, pp. 1–42, 2012.

[46] Y.-R. Luo, *Comprehensive Handbook of Chemical Bond Energies*, vol. 58. CRC Press, Mar. 2007.

[47] C. Kittel, *Introduction to solid state physics*. Wiley, 2005.

[48] W. P. Davey, "Precision measurements of the lattice constants of twelve common metals," *Physical Review*, vol. 25, pp. 753–761, 1925.

[49] P. Haas, F. Tran, and P. Blaha, "Calculation of the lattice constant of solids with semilocal functionals," *Physical Review B*, vol. 79, p. 085104, Feb. 2009.

[50] P. Jensen, X. Blase, and P. Ordejón, "First principles study of gold adsorption and diffusion on graphite," *Surface Science*, vol. 564, pp. 173–178, 2004.

[51] L. Ferrighi, Y.-x. Pan, H. Grönbeck, and B. r. Hammer, "Study of Alkylthiolate Self-assembled Monolayers on Au(111) Using a Semilocal meta-GGA Density Functional," *The Journal of Physical Chemistry C*, vol. 116, pp. 7374–7379, Apr. 2012.

[52] N. E. Singh-Miller and N. Marzari, "Surface energies, work functions, and surface relaxations of low-index metallic surfaces from first principles," *Physical Review B*, vol. 80, p. 235407, Dec. 2009.

[53] W. Tyson and W. Miller, "Surface free energies of solid metals: Estimation from liquid surface tension measurements," *Surface Science*, vol. 62, pp. 267–276, Jan. 1977.

[54] R. Nuzzo, B. Zegarski, and L. Dubois, "Fundamental studies of the chemisorption of organosulfur compounds on gold(111). Implications for molecular self-assembly on gold surfaces," *Journal Of The American Chemical Society*, 1987.

[55] L. H. Dubois and R. G. Nuzzo, "Synthesis, structure, and properties of model organic surfaces," *Annual Review of Physical Chemistry*, vol. 43, pp. 437–463, 1992.

[56] D. S. Karpovich and G. J. Blanchard, "Direct Measurement of the Adsorption Kinetics of Alkanethiolate Self-Assembled Monolayers on a Microcrystalline Gold Surface," *Society*, pp. 3315–3322, 1994.

[57] L. Zhao, R. Najafabadi, and D. J. Srolovitz, "Finite temperature vacancy formation thermodynamics: local harmonic and quasiharmonic studies," *Modelling and Simulation in Materials Science and Engineering*, vol. 1, pp. 539–551, July 1993.

[58] W. Triftshäuser and J. D. McGervey, "Monovacancy formation energy in copper, silver, and gold by positron annihilation," *Applied Physics*, vol. 6, pp. 177–180, 1975.

[59] P. Jongenburger, "Energy of Formation of Vacancies in Copper and Gold," *Phys. Rev.*, vol. 106, pp. 66–69, 1957.

[60] C. P. Flynn, J. Bass, and D. Lazarus, "The vacancy formation and motion energies in gold," *Philosophical Magazine*, vol. 11, no. 111, 1965.

[61] C. Meechan and R. R. Eggleston, "Formation energies of vacancies in copper and gold," *Acta Metallurgica*, vol. 2, no. 5, pp. 680–683, 1954.

[62] L. Verlet, "Computer "experiments" on classical fluids. I. Thermodynamical properties of Lennard-Jones molecules," *Physical Review*, vol. 159, pp. 98–103, 1967.

[63] D. Krüger, H. Fuchs, R. Rousseau, D. Marx, and M. Parrinello, "Pulling Monatomic Gold Wires with Single Molecules: An Ab Initio Simulation," *Physical Review Letters*, vol. 89, p. 186402, Oct. 2002.

[64] Y. Xue, X. Li, H. Li, and W. Zhang, "Quantifying thiol-gold interactions towards the efficient strength control.," *Nature communications*, vol. 5, p. 4348, 2014.